© 2018. Published by The Company of Biologists Ltd | Journal of Experimental Biology (2018) 221, jeb166512. doi:10.1242/jeb.166512

RESEARCH ARTICLE

Biomechanics of omnidirectional strikes in flat spiders

Yu Zeng[1,2,*,‡] and Sarah Crews[3]

ABSTRACT

Many ambush predators attack prey using rapid strikes, but these strikes are typically only anteriorly directed. However, a predator may attack laterally and posteriorly oriented prey if it can couple the strikes with rapid body reorientation. Here, we examined omnidirectional strikes in flattie spiders (Selenopidae), a group of sit-and-wait ambush predators found on open surfaces. These spiders attack prey throughout their entire peripheral range using rapid strikes that consist of rapid translation and rotation toward the prey. These spiders ambush with radially oriented, long, laterigrade legs in a ready-to-fire status. Once prey is detected, the spider maneuvers toward it using a single flexion of the legs closest to the prey, which is assisted by 0–3 extension strides by the contralateral legs. The within-stance joint actions by a few legs generate a large resultant force directed toward the prey and a large turning moment. Furthermore, the turning speed is enhanced by rapid midair leg adductions, which effectively reduce the spider's moment of inertia during angular acceleration. Our results demonstrate a novel hunting behavior with high maneuverability that is generated with effectively controlled reconfigurations of long, laterigrade legs. These results provide insights for understanding the diversity of animal legs and developing highly maneuverable multi-legged robots.

KEY WORDS: Arthropod, Legged locomotion, Maneuverability, Predator–prey interaction

INTRODUCTION

Maneuvering is essential to locomotion and plays an important role in the behavior of legged animals. Most studies of legged maneuvers have focused on turning during forward walking and running (e.g. turning maneuvers in running cockroaches; Jindrich and Full, 1999). In general, turns are generated by laterally asymmetric forces that deflect the animal's mean heading, and maintaining the alignment of the body axis with the heading direction is essential for resuming a straight path after turning. For multi-legged animals, the forces and moments required for turning should be generated through well-coordinated asymmetric gaits. Moreover, effective regulation of the position of the center of pressure increases the efficiency and stability of turning movements (Full et al., 2002). For example, running cockroaches adopt bilaterally asymmetric gaits to achieve ∼90 deg turns within ∼5 strides with an anteriorly positioned center of pressure (Jindrich and Full, 1999). The typical leg configuration of arthropods – multiple legs in a sprawled posture – provides high static stability, yet specific coordination may be required for rapid, transient maneuvers. The jointed design of arthropod legs enables controlled changes of functional length (i.e. the length of a vector from the center of mass to the point of foot contact), which have been shown to enable asymmetric stride length during turning maneuvers (e.g. cockroaches; Franklin et al., 1981; Jindrich and Full, 1999). In the context of maneuvering, a relatively underexplored aspect of jointed legs is the ground reactions during stance. Depending on the joint configurations, controlled deformation of multi-jointed legs anchored on the substrate can generate ground reaction forces and moments that are unachievable by otherwise unjointed appendages (i.e. parapodia; Manton, 1973; Full, 1997; Wootton, 1999). Furthermore, active reconfiguration of leg postures can potentially be used for changing the animal's moment of inertia and thus to regulate the state of rotation.

Predator–prey interactions are useful for studying animal maneuvers. The arms race between predator and prey drives the evolution of extreme maneuverability. For predators, outcompeting prey in speed and maneuverability is favored by selection (Moore and Biewener, 2015). Many ambush predators capture or attack prey by rapidly striking at speeds that exceed the prey's escape responses. Strikes are typically rapid forward movements of the body or appendages powered by the sudden release of a large amount of energy. These strikes have a limited angular range of attack and only target prey directly anterior to the predator (e.g. anteriorly directed strikes in a mantis shrimp and a rattlesnake; deVries et al., 2012; Kardong, 1986). Nevertheless, the attack ranges can be enhanced if the predator can couple linear strike movements with rapid body reorientation.

The flattie spiders (family: Selenopidae) are nocturnally active sit-and-wait ambush predators. They ambush on open surfaces in diverse habitats (e.g. tree trunks and rock surfaces) (Crews et al., 2008; Crews and Harvey, 2011). These spiders have long legs that are characterized by a ∼90 deg supination at the leg base (i.e. trochanter joint) so that the prolateral surface is approximately dorsal. This laterigrade postural configuration presumably allows the leg to change functional length and orientation in the fore–aft and lateral directions. This posture configuration means that the bulk of the range of motion of, for example, the tarsus, is aligned with the plane of the substrate rather than being more vertically or dorsoventrally oriented. In addition to standard spider sensory organs on the legs, selenopid spiders have large posterior lateral eyes, suggesting a wide field of view that may allow prey detection from anterior, lateral and posterior directions (Fig. 1). These spiders' legs are radially oriented, including when preparing to ambush. Preliminary observations showed that these spiders were capable of capturing prey approaching from any direction within the entire peripheral range. In the context of these ambush attacks, the predator needs to achieve rapid body maneuvers toward the prey, thus requiring effective mechanisms

[1]School of Natural Sciences, University of California, Merced, 5200 N. Lake Road, Merced, CA 95343, USA. [2]Department of Integrative Biology, University of California, Berkeley, 3040 Valley Life Sciences Bldg #3140, Berkeley, CA 94720-3140, USA. [3]Department of Entomology, California Academy of Sciences, Golden Gate Park, 55 Music Concourse Drive, San Francisco, CA 94118, USA.
*Present address: Room 347, Science and Engineering Building 1, UC Merced, 5200 N. Lake Rd., Merced, CA 95343, USA.

‡Author for correspondence (yzeng7@ucmerced.edu)

Y.Z., 0000-0002-2651-227X

Received 17 July 2017; Accepted 10 January 2018

Journal of Experimental Biology (2018) 221, jeb166512. doi:10.1242/jeb.166512

List of abbreviations and symbols

AAL	aerial adduction leg
COM	center of mass
CTF	coxa–trochanter–femur
d_S	body translation distance through the strike maneuver
FP	femur–patella
G	gravitational acceleration
H	coordinate frame
I	moment of inertia
IFL	inside flexion leg
L_b	body length
L_F	functional length
m	mass
MI	maneuver index
MMR	maneuver momentum ratio
OEL	outside extension leg
r_I	rate of change of moment of inertia
T	strike period
v	translational velocity
ΔL_F	degree of leg functional length change (strain of leg abduction/adduction)
θ_S	angle of body reorientation through the strike maneuver
ω	rotational velocity

for simultaneously generating linear and angular momenta using coordinated leg movements. The dynamics of the ambush turns should therefore differ from the aforementioned turning during forward running. Here, we propose two primary hypotheses regarding the biomechanical features for strike maneuvers in selenopid spiders: (1) the spiders adopt gait configurations optimized for driving strike maneuvers with long, laterigrade legs (e.g. generation of highly asymmetric lateral forces); (2) the long, laterigrade legs are effective for driving these ambush turns with the freedom of motion in the lateral direction (e.g. leg shape change for both generating ground reaction forces during stance and regulating whole-spider inertia). Under controlled lab conditions, we filmed at high speed six species of flattie spiders striking prey approaching from different directions on a horizontal surface and examined the 3D body and leg kinematics to understand the underlying mechanisms.

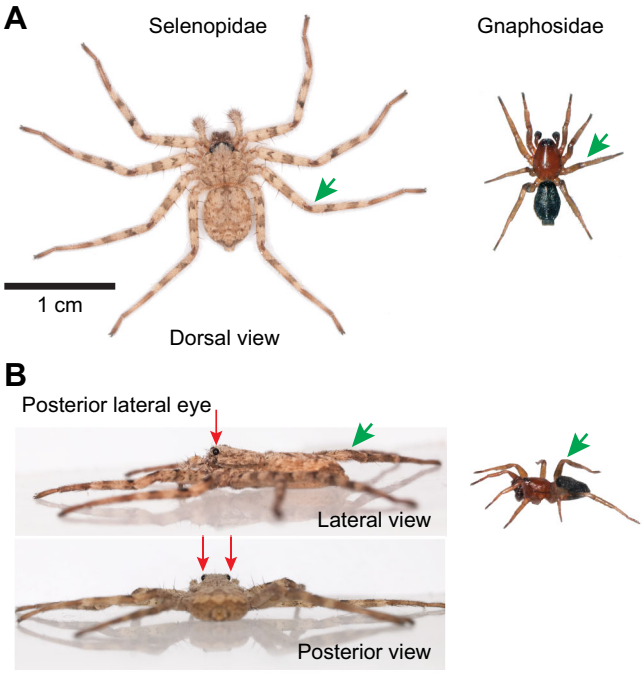

Fig. 1. Overview of the body plan and laterigrade legs in selenopid spiders, demonstrated by *Selenops debilis*. (A) Dorsal view. (B) Lateral and posterior views. Selenopid legs are characterized by a ~90 deg supination at the leg bases and can achieve wide ranges of lateral motion within the frontal plane in contrast to legs in which the morphologically dorsal surface is directed dorsally (demonstrated with a gnaphosid spider, right). Green arrows indicate femur–patella joints. Red arrows indicate the large posterior lateral eyes.

MATERIALS AND METHODS

Spider husbandry and morphometrics

Spiders were collected in the field and transferred to the lab (species, taxonomic authority, origin and number of individuals: *Selenops mexicanus*, Keyserling 1880, Mexico, N=2; *Selenops radiatus*, Latreille 1819, Namibia, N=1; *Selenops bifurcatus*, Banks 1909, Costa Rica and Nicaragua, N=3; *Selenops debilis*, Banks 1898, Arizona, USA, N=7; *Selenops wilsoni*, Crews 2011, Jamaica, N=4; *Selenops insularis*, Keyserling 1881, Elbow Cay, Bahamas, N=3; unidentified juveniles, N=4). All individuals were kept in plastic vials at room temperature (22–25°C). Spiders were fed small prey (e.g. fruit flies or nymphal crickets) once per week. To sample mass distribution, the spider body was divided into 26 sections, including cephalothorax, abdomen, and eight legs, each with three sections (Fig. 2A). The mass of each section was sampled from deep-frozen specimens (N=10). All specimens have been deposited in the California Academy of Sciences.

Experimental setup and motion digitization

Filming was conducted at a controlled temperature (25–28°C). During each trial, a single spider was transferred into an uncovered plastic arena (20×30×10 cm, width×length×depth) with Fluon-coated inner walls and a horizontal floor. We used fishing line or bursts of air to compel the spider to move to the center of the arena floor. Two synchronized high-speed video cameras (1280×1024 pixels, 500–1000 Hz; HiSpec1, FasTec Imaging, San Diego, CA, USA) were set up to film directly overhead and laterally. Halogen bulbs were used to enhance environmental luminance, but direct illumination onto the spiders was avoided. For each trial, a single cricket (body length 2–5 mm) was released and allowed to walk freely near the spider. The release points of the prey were biased to the posterior direction to capture the strikes with wider turns. Cameras were post-triggered after the spider captured the prey.

Motion digitization was conducted using MTrackJ v. 1.5.0 with ImageJ (http://www.imagescience.org/meijering/software/mtrackj; Schindelin et al., 2015) tracking 36 landmarks (Fig. 2A). Three-dimensional reconstruction was conducted using commercial software (ProAnalyst, Xcitex Inc., Woburn, MA, USA). To assess digitizing error, a single trial was digitized 5 times, and the standard deviation of each landmark from these five trials was <0.01% in all coordinates. We used a quintic spline function to fit the positional data of each landmark, and the averaged root mean square error (Walker, 1998) of the positional data was <1% of the absolute values of mean data along all axes.

Strike maneuver behavior and body kinematics

Our biomechanical analyses treated the spider as a system of rigid bodies connected by joints. All kinematic data and calculations followed a standard left turn by the spider. Data from trials in which

Journal of Experimental Biology (2018) 221, jeb166512. doi:10.1242/jeb.166512

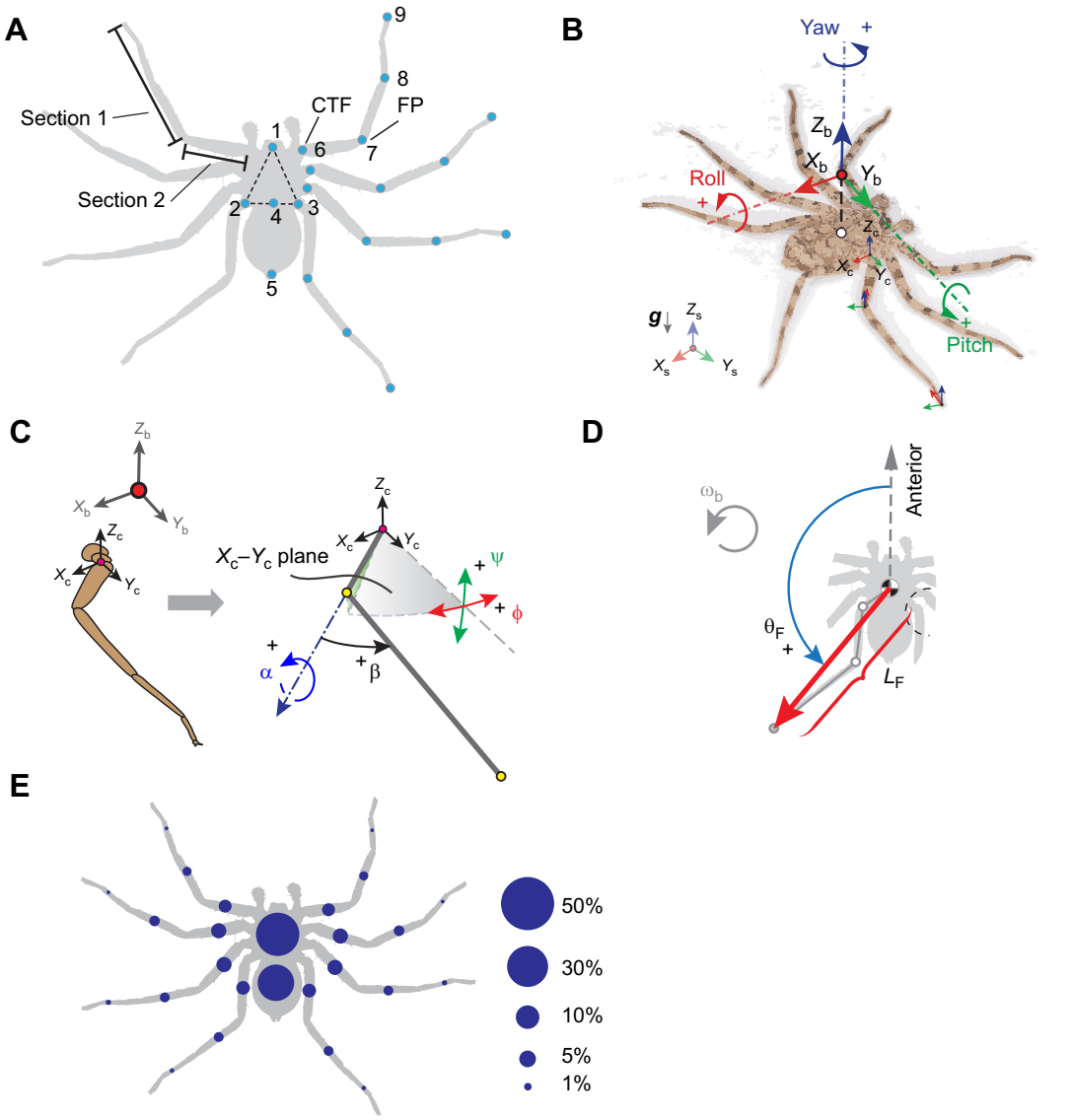

Fig. 2. Morphometrics and kinematic configurations. (A) *Selenops* spider body plan in dorsal view. Morphological landmarks for motion reconstruction are marked by blue dots. Landmarks for the body-fixed frame: (1) midpoint of the front of the cephalothorax; (2,3) coxa of the left and right leg IV, respectively; (4) posterior middle of the cephalothorax; (5) distal end of the abdomen. Landmarks for the legs: (6) combination of coxa–trochanter–femur (CTF) joint; (7) femur–patella (FP) joint; (8) tibia–metatarsus joint; (9) tarsus tip. Each leg was modeled as two sections: the combination of patella, tibia, metatarsus and tarsus (section 1) and the femur (section 2). (B) Configuration of the body-fixed coordinate frame (X_b, Y_b, Z_b), elevated in the +Z direction for clarity. Coxa- and section-fixed frames for legs are indicated on right leg III (X_c, Y_c, Z_c and X_S, Y_S, Z_S, respectively). (C) Configuration of leg posture angles demonstrated with leg III. Left: the coxa-fixed coordinate frame has principal axes parallel to those of the body-fixed frame. Right: four angles describe leg posture: ϕ, sweep angle; ψ, elevation angle; α, rotation angle; β, FP joint angle. (D) Configuration of 'functional leg' representation in the horizontal plane. L_F, functional length; θ_F, orientation with respect to the anterior of the spider, with counter-clockwise as the positive direction; ω_b, reorientational rotation of body. (E) Schematic demonstration of mass distribution based on average mass percentages of body and leg sections.

the spider performed right turns were mirrored about the sagittal plane. All kinematic analyses were conducted using custom-written MATLAB scripts (R2015b, MathWorks, Natick, MA, USA), which are available upon request.

Here, 'body' represents the combination of the cephalothorax and the abdomen. A body-fixed frame (H_b) was set at the midpoint of both coxae IV and was defined by an X_b-axis parallel to the body longitudinal axis, a Z_b-axis that is dorsally oriented, and a Y_b-axis that is the cross-product of X_b and Z_b (Fig. 2B). Body kinematics was described based on the motion of H_b with respect to a spatial frame (H_S), the Z_S-axis of which is vertical and perpendicular to the substrate plane. Following Murray et al. (1994), the translational velocity of H_b was calculated as:

$$v_b = -\dot{R}_b R_b^T p_b + \dot{p}_b = [v_{b,x}, v_{b,y}, v_{b,z}]^T, \quad (1)$$

where R_b and p_b are the rotational matrix and the position of H_b with respect to H_S, respectively. The trajectory of the spider's center of mass (COM) was estimated based on the positions of point masses associated with each body and leg sections, and the position of the COM with respect to H_S was calculated as:

$$p_B = m_B^{-1} \sum_{i=1}^{13} m_i p_{m_i}, \quad (2)$$

Journal of Experimental Biology

where m_B and m_i are total mass and section mass, respectively, and p_{m_i} is the spatial position of section mass. The position of the COM with respect to H_b was calculated as:

$$p_{B-b} = R_b p_B^T + p_b. \quad (3)$$

Velocities of three principal rotations of H_b were calculated as:

$$\omega_b = (\dot{R}_b R_b^T)^V = [\omega_{b,x}, \omega_{b,y}, \omega_{b,z}]^T. \quad (4)$$

Body rotations were also described using 'axis-angle' representation:

$$\omega_b = \hat{e}_b \cdot |\omega_b|, \quad (5)$$

where $\hat{e}_b = [\hat{\omega}_{b,x}, \hat{\omega}_{b,y}, \hat{\omega}_{b,z}]$ represents the direction of the rotational axis with respect to H_b, and $|\omega_b|$ is the magnitude of overall rotation.

In the context of a strike maneuver, reorientation is defined as the rotation of body longitudinal axis about a vertical axis. Reorientational rotation can thus be described by the projection of the X_b-axis on the horizontal plane. The maneuvering phase was defined as the interval during which the spider performs one continuous rotation and finishes with completed decelerations of both translation and rotation. Also, the duration of the maneuvering phase was used as the strike period in our analyses. The linear distance of strike (d_S) was calculated based on the horizontal component of spider COM translation. The angle of reorientation (θ_S) was calculated as the angular distance between a spider's initial anterior direction and final anterior direction.

Leg behavior and kinematics

Three basic leg roles were categorized based on behaviors during maneuvering phases: (1) inside flexion leg (IFL) – legs inside of the rotation that flex during stance; (2) outside extension leg (OEL) – legs outside of the rotation that extend during stance, and one OEL may perform multiple strides; (3) aerial adduction leg (AAL) – legs on either side of the rotation that swing mid-air throughout the maneuvering phase (see below). These leg behaviors were identified by examining whether each leg was in stance (i.e. anchored on the substrate) or swinging mid-air throughout the strikes, and the differences between these categories were obvious given the asymmetric kinematics and adduction (see Movie 1).

Leg kinematics were described by modeling each leg as two rigid sections. The combination of the coxa–trochanter–femur (CTF) joints was treated as a spherical joint, and the femur–patella joints were treated as revolute joints. A section-fixed frame (H_x) was set at the distal end of each leg section, with the X_x-axis in the longitudinal direction, the Y_x-axis parallel with the X_b–Y_b plane, and the Z_x-axis as the cross-product of X_x and Y_x. Leg kinematics was primarily described using four angles. The posture and orientation of the femur was described by sweep (ϕ), elevation (ψ) and rotation (α) angles based on the relative orientation of the femur-fixed frame to a coxa-fixed frame (H_c), the principal axes of which were parallel with those of H_b. The FP joint angle (β) was the intersection angle between two leg sections (Fig. 2C).

The stance legs drove strike maneuvers through controlled joint rotations during stance. The kinematics of leg reconfigurations were described based on length and orientation of the vectors from the spider COM to each tarsus tip ('functional leg'; Fig. 2D), and the reconfiguration dynamics were represented by temporal variations in functional length (L_F) and orientation with respect to the spider's anterior direction (θ_F).

Whole-spider inertial dynamics

Ground reaction forces and moments were evaluated by modeling the spider as a system of rigid sections, each represented by a point mass located at its geometric center (Fig. 2E). We ignored any potential damping between joints and elastic energy storage in muscles. A COM-fixed frame (H_B) was used for all calculations of angular momentum, with all axes parallel to those of H_b. For each principal rotation, the moment of inertia (I) about spider COM was calculated as:

$$I = \sum_{i=1}^{25} r_i^2 m_i, \quad (6)$$

where m_i is the mass of each section and r_i is the vector from the spider COM to section mass. Angular momentum was calculated as:

$$M_R = \sum_{i=1}^{25} r_i \times m_i v_i, \quad (7)$$

where $v_i = \omega_i \times r_i$ is the linear velocity of section mass with respect to H_B. Instantaneous torques were calculated as the time derivative of M_R. Linear momentum and forces were estimated based on the translational dynamics of the COM. Translational work was calculated as $W_T = \int v_b f_G dt$, where f_G is the ground reaction force. Rotational work was calculated as $W_R = \int \omega_b \tau_G dt$, where τ_G is the ground reaction torque.

Assessment of maneuverability

The ratio of angular momentum to linear momentum during the strike (maneuver momentum ratio, MMR) was calculated as:

$$\mathrm{MMR} = \frac{\bar{M}_R}{\bar{M}_T} = \frac{I_H \bar{\omega}_B}{m \bar{v}_B}, \quad (8)$$

where $\bar{M}_R$ and $\bar{M}_T$ are average angular and linear momentum about the spider COM, respectively, I_H is the moment of inertia for reorientational rotation (i.e. about a rotational axis perpendicular to the substrate), $\bar{\omega}_B$ is the mean speed of reorientational rotation, m is the mass, and $\bar{v}_B$ is the mean COM linear velocity.

We defined the ratio of body reorientation angle to the deflection of COM linear speed during a single stance as the maneuver index (MI) and calculated it as:

$$\mathrm{MI} = \frac{\Delta\theta_R}{\Delta\theta_T}, \quad (9)$$

where $\Delta\theta_R$ is the angle of body reorientation and $\Delta\theta_T$ is the change in the heading of COM. For example, a large MI represents a wide-angle body reorientation with a small change in the direction of heading. Here, the MI is used to describe the body maneuver during leg stance. Although the formula for MI is the same as that for the leg effectiveness number used in turning during forward running (Jindrich and Full, 1999), these two numbers are in two different behavioral contexts (i.e. strike maneuvers versus forward running).

Statistical analyses

Four types of statistical analyses were used in this study. (1) Descriptive statistics for morphology, behavior and kinematics. Because of the limited sample size for each species and unrepeatability of strikes to the same prey location, we omitted the potential interspecific variations of strike behavior. All calculations of means and standard deviations were based on data from all individuals. (2) Correlational analyses for prey distance and strike speeds. We used a multiple regression model to analyze how

linear and angular strike speeds are correlated with prey distance and body size. (3) Correlation between leg kinematics and body maneuvers. We used generalized linear models to analyze the linear correlations between leg kinematics (i.e. changes in length and orientation of functional legs) and body kinematics (e.g. linear and angular distances traveled during strikes). (4) Correlation between gait configuration and prey location. We used multiple regression models to examine how the number of strides and choices of leg pairs for both IFL and OEL are potentially correlated with the linear and angular distances of prey. The results are shown in the Results ('Prey-aiming gait configuration') and Appendix ('Gait configuration'). All statistical analyses were conducted using custom-written R (http://www.R-project.org) scripts (deposited in the Open Science Framework repository: https://osf.io/h9b4t/?view_only=bd3fa03865ad4fcd8b887b778c474c25).

RESULTS

Morphology

Spider body length ranged from 0.5 to 1.4 cm and total mass ranged from 19 to 279 mg (N=20 individuals). Leg length was 1.3–2.0 times the body length, and an average of 44% of the total mass was associated with the legs (Tables S1 and S2).

Maneuvering kinematics of omnidirectional strikes

The strikes were rapid turn-and-reach maneuvers directed toward the prey, which was then grasped by legs I and II of the spider. The spiders successfully struck prey within 40–116 ms, and prey location was distributed within a 5 body length radius of the full peripheral range relative to the COM. The strike ranges produced by the remarkable combination of angular and linear attack were greater than the forward-only strike ranges typically seen in ambush predators (e.g. mantis shrimp and viper snakes; Fig. 3; Table S3, Movie 1).

The strike maneuvers consisted of a transition from a static initial position to a static end position through rapid body translation and reorientation that turned the anterior of the spider toward the prey. These strike maneuvers were initiated by bursts of linear and angular accelerations at the COM, which were followed by decelerations toward the end of the strike. The spider COM traveled along slightly curved trajectories from the initial position toward the prey location (curvature 2.5±6.5 cm^{-1}, mean±s.d., N=32 trials). The peak linear acceleration was 23.0±1.9 m s^{-2} (mean±s.e.m.; 2.3±0.2 times gravitational acceleration $\boldsymbol{g}$; range 8.5–43.6 m s^{-2}, or 0.9–4.5 $\boldsymbol{g}$). Mainly consisting of yaw (Fig. S1), the body reorientation showed acceleration ranging from 3.8×10^4 to 3.5×10^5 deg s^{-2}, with the peaks occurring earlier than that of the linear acceleration (Fig. 4A–C). Both linear and angular components of body maneuver showed deceleration during the later stage of strikes. In the most extreme cases, the spiders turned >100 deg along the horizontal plane to strike prey that were in the posterior lateral direction or directly behind, with average rotational speeds of 2000–3000 deg s^{-}, which is among the fastest turning maneuvers documented in arthropods (Fig. 4D; see also Table S4).

Furthermore, strike maneuver speeds were correlated with prey distance. Specifically, greater linear and angular speeds were generated for striking farther and more posteriorly oriented prey. In addition, smaller spiders exhibited greater speeds than larger ones (Fig. 4E,F; Table S5). Accordingly, the ratio of total generated angular momentum to linear momentum scaled with the ratio of the prey's angular distance to linear distance (see Appendix, 'Scaling of maneuver momentum ratio'). Amongst all trials, the maximum body mass-specific rotational work was ∼1.2 J kg^{-1} and the maximum mass-specific translational work was ∼5.2 J kg^{-1}.

Prey-aiming gait configuration

To understand the underlying mechanisms of these strikes, we first examined which legs directly interacted with the substrate. We found that the radially symmetric leg alignment during ambush allowed the spiders to configure a highly asymmetric, prey-aiming gait each time. When initiating the strikes, the 1–2 legs that were closest to the prey immediately anchored on the substrate and performed a rapid flexion motion of the FP joint (e.g. anchor and pull-in; Fig. 5A–C). These stance legs are positioned inside of the rotation and are designated 'inside flexion leg' (IFL). The action of IFL may be assisted by 1–3 contralateral legs, which performed within-stance extensions (e.g. anchor and push) during 1–5 non-overlapping strides. These stance legs outside of the rotation are designated 'outside extension leg' (OEL). Overall, 9 of 32 trials (∼30%) were driven by IFL only (i.e. only IFL was in contact with the substrate; Fig. S5), and the other 22 trials were driven by both the IFL and OEL. By contrast to the consistent choice of IFL aimed at the prey, the choice of OEL was highly variable (see Appendix, 'Gait configuration').

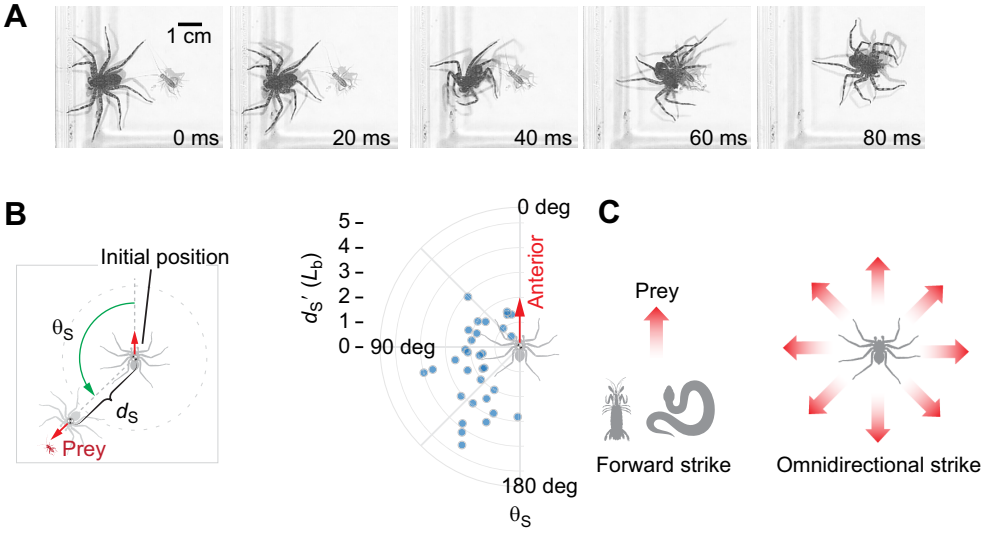

Fig. 3. Omnidirectional strike performance. (A) A sequence of *Selenops bifurcatus* capturing posteriorly oriented prey within 80 ms. (B) Left: configuration of strike maneuver performance: d_S, linear distance traveled by center of mass (COM); θ_S, angle of body reorientation relative to the initial orientation. Right: distribution of strike distance [normalized to body length; $d_S'(L_b)$] and reorientation angle (θ_S), plotted with respect to a polar coordinate frame centered at the initial COM location (N=32 trials). (C) Schematic comparison of the range of attacks between omnidirectional strikes and forward strikes (see also Table S3).

Journal of Experimental Biology (2018) 221, jeb166512. doi:10.1242/jeb.166512

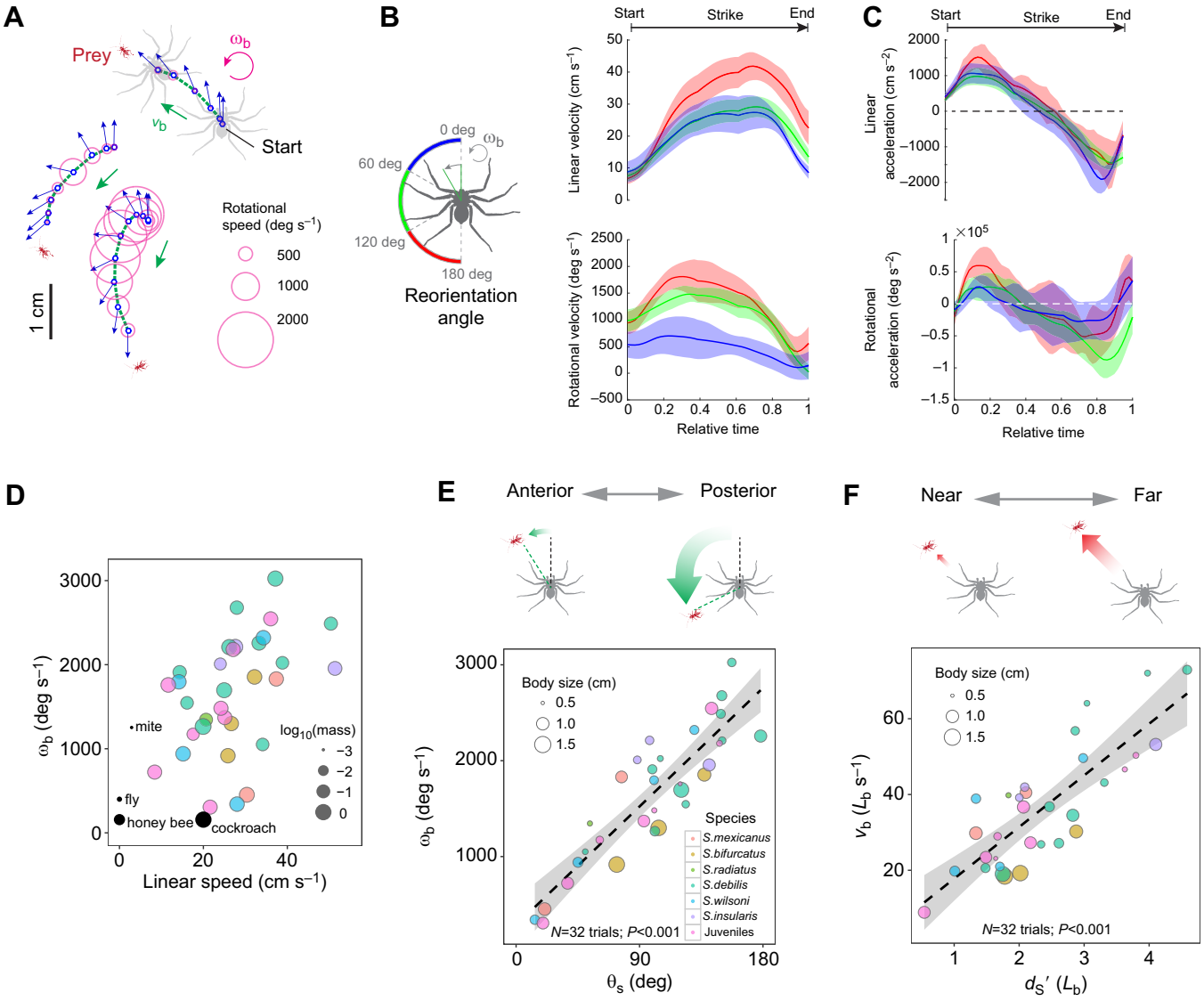

Fig. 4. Maneuver kinematics of omnidirectional strikes. (A) Three COM trajectories of strike maneuvers in top view (time interval, 8 ms), showing faster body rotations are performed when striking more posteriorly oriented prey. Circle size denotes the speed of reorientational rotation. ω_b, reorientational velocity of COM; v_b, velocity of COM. (B) Linear speed of COM and body reorientational speed throughout the strikes. Binning was used to demonstrate the variation of body kinematics with respect to the angular distance of the prey (0–60 deg, *N*=7 trials; 60–120 deg, *N*=13; 120–180 deg, *N*=12). (C) COM linear acceleration and rotational acceleration of the body frame throughout the strikes. For B and C, the lines and shaded areas indicate means±s.d., with different colors representing the three ranges of total reorientation angle. Data are based on translational and rotational movements within the horizontal plane (see Materials and methods). Peak angular acceleration averages 1.6×10^5±1.4×10^4 deg s^{-2} (mean±s.e.m.). (D) An overview of the reorientational speed (ω_b) and linear speed of selenopid spider ambush turns (colored dots) compared with turning maneuvers in four different arthropods (black dots; tight turns for fly and honey bee, and turning during forward runs for mite and cockroach). Colors represent different species (see E). The size of the points represents log-transformed body mass. See Table S4 for more details. (E) Positive correlation between reorientation angle (θ_S) and mean reorientational speed (ω_b). (F) Positive correlation between COM translational speed (v_b) and the linear distance (d_S) of prey to the initial COM position. L_b, body length. For E and F, the arrow size in schematic figures represents the magnitude of speed, the trend lines are based on linear regression models, and shaded areas denote s.e.m. Kinematics is based on a left-turn configuration.

Kinematics of stance legs

We further explored the kinematics of the reconfigurations of stance legs and how they correlate with body maneuvers. Using the functional leg representation, we found wide ranges of leg motion in the horizontal plane (Fig. 6A; Movie 2). The IFL's actions consisted of functional length reduction (i.e. adductions) by 49±18% (mean± s.d., *N*=32 IFL actions), which corresponds to 0.4–3 times body length, and forward rotations (amplitude 0–60 deg; angular speed 0–2200 deg s^{-1}). The OEL's actions consisted of functional length increase (i.e. abductions) by 16±15% (*N*=24 OEL actions) and backward rotations (amplitude 0–25 deg; speed 0–3000 deg s^{-1}) (Fig. 6C,D). These wide ranges of motion in the lateral direction by stance legs support our second hypothesis, that they are effective for driving ambush turns. The foot positions of IFL and OEL were maintained in the leading and trailing positions, respectively, of the heading of the COM.

Also, the stance pattern was highly asymmetric between IFL and OEL. IFL actions were associated with relatively long stance periods (32±12 ms), while OEL had relatively short stance periods (12±6 ms). These kinematic patterns are primarily associated with the actions and independent of the choice of leg pairs (see Appendix, 'Kinematics of stance legs'). The temporal percentage of

Journal of Experimental Biology (2018) 221, jeb166512. doi:10.1242/jeb.166512

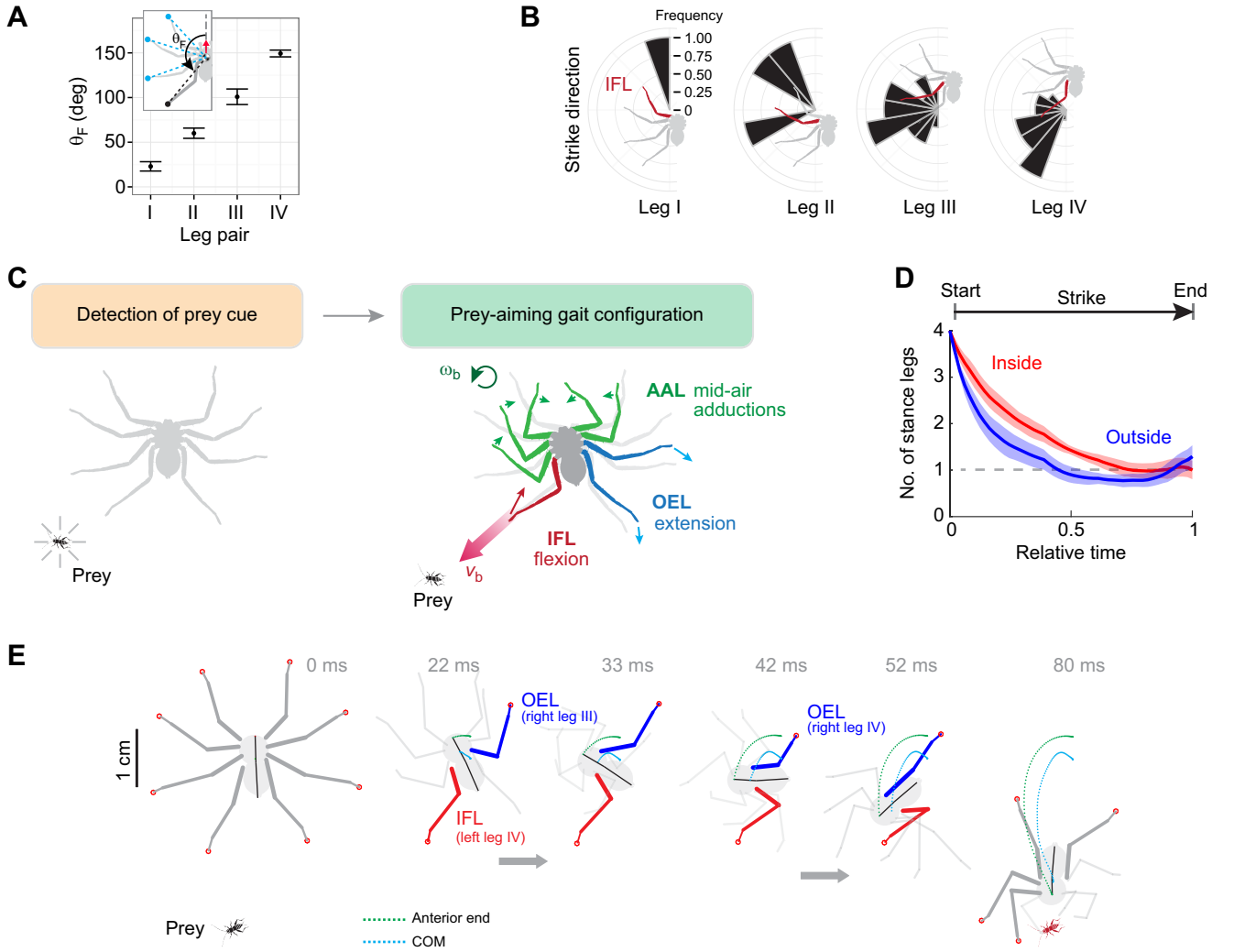

Fig. 5. Prey-aiming gait configuration. (A) Initial leg orientation (θ_F) during ambushing. Values are means±s.d. (B) Polar histograms of the mean strike directions performed with different inside flexion legs (IFL; i.e. the legs inside of the rotation that flex during stance), showing the correlation between IFL orientation and strike direction. (C) Schematic demonstration of the general gait configuration for striking posteriorly oriented prey. To strike and reorient towards prey, the spider pulls with the IFL, pushes with its outside extension legs (OEL; i.e. legs outside of the rotation that extend during stance), and adducts other legs, or 'aerial adduction legs' (AAL; i.e. legs on either side of the rotation that swing mid-air throughout the strike maneuver). Arrows indicate leg movements relative to the body. (D) Variation of the mean number of stance legs throughout the strike period (N=32 trials). (E) A full strike maneuver sequence in top view, where the spider body and legs are represented by line segments based on 3D kinematics data. Two mid-maneuver intervals (22–33 ms and 42–52 ms) show that a single IFL (left leg IV) drives the strike maneuver with two OEL (right legs III and IV). Mid-maneuver stance legs are shown in color. Red circles on tarsi represent substrate contact. Kinematics is based on a left-turn configuration.

leg stance period to total strike period was 53.4±16.2% (mean±s.d.) for IFL and 18.7±12.7% for OEL. Overall, the IFL actions correspond to longer body translation distance and wider body rotation angle than OEL actions (Fig. 6E). The MI (i.e. the ratio of body reorientation angle to the deviation of COM heading per stance) was −7.38 to 26.09 for IFL and −4.66 to 20.13 for OEL.

Further analyses also showed that the kinematics of body translation and rotation are correlated with the reconfiguration of stance legs. The overall linear distance traveled by the COM was positively correlated with the degree of IFL adduction, and the overall body reorientation was correlated with the angles of rotation of both the IFL and OEL (Fig. 7).

Enhancement of rotation speed by leg adduction

All legs performed rapid adduction when initiating strikes. The 2–7 non-stance legs that performed mid-air adduction were designated aerial adduction legs (AAL). The AAL pulled in and lifted off, swung mid-air, and extended and touched down as the strike ended. These rapid leg adductions largely enhanced the speed of body reorientation. On average, the rapid leg adductions induced a 25–38% reduction of the spider's mass moment of inertia for reorientational rotation by the end of the initial ∼40% of the strike period (T) (Fig. 8A). This rapid reduction of moment of inertia can amplify the effect of reorientational rotation generated by the stance legs. Based on a simplified model assuming consistent angular impulse during the acceleration phase (i.e. 0–0.4 T; see Appendix, 'Derivation of rotational speed enhancement by leg adductions'), we estimated that the spiders effectively enhanced the reorientational speed by 3–8 times with leg adductions compared with a situation without leg adduction (Fig. 8B).

DISCUSSION

Generation of omnidirectional strikes

Our study showed that the selenopid spiders generate rapid strikes to attack prey approaching from any direction. Various prey cues may be

Journal of Experimental Biology (2018) 221, jeb166512. doi:10.1242/jeb.166512

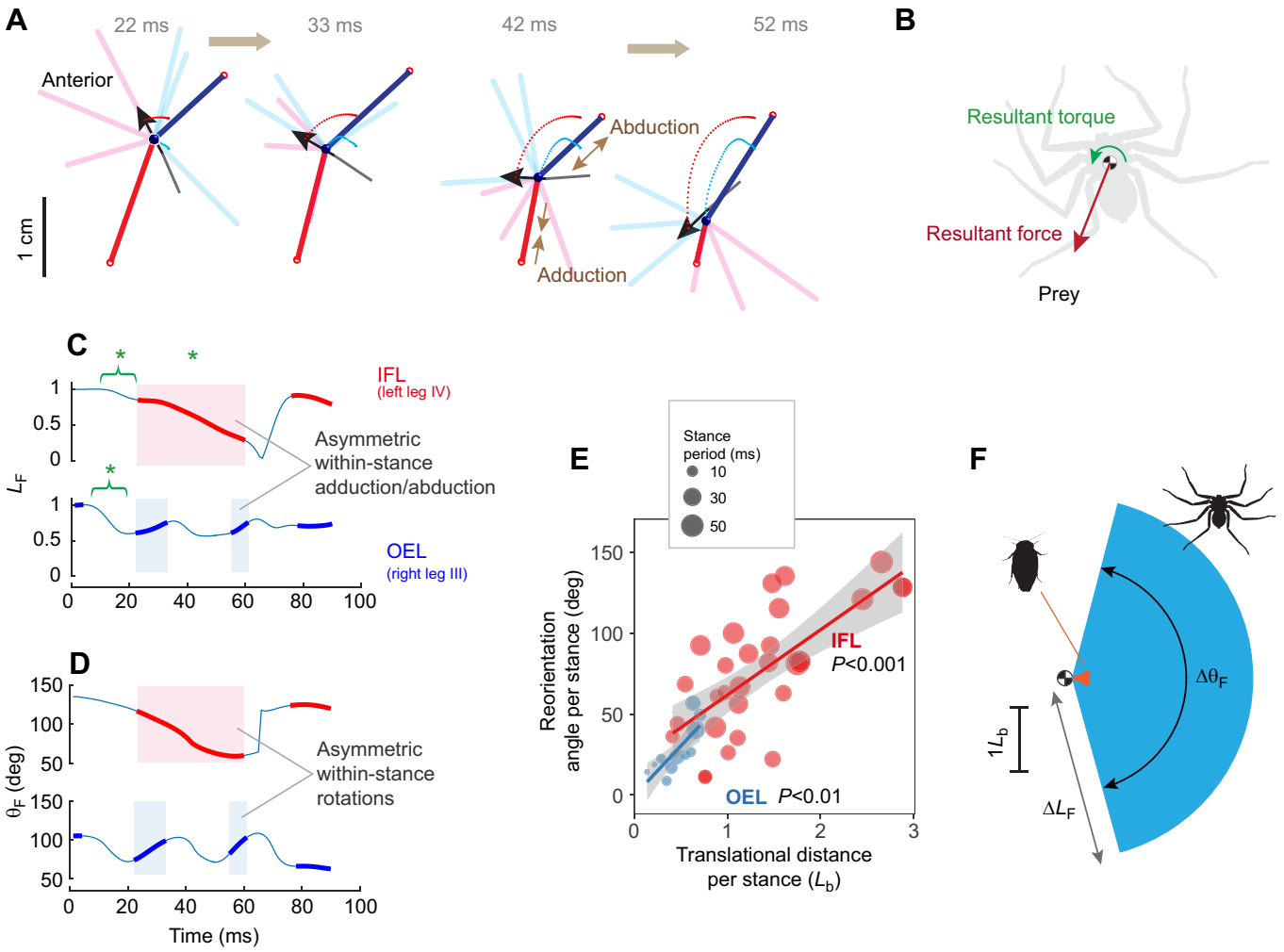

Fig. 6. Kinematics of controlled leg reconfigurations underlying omnidirectional strikes. (A) A sequence of a strike maneuver (Fig. 5E) in functional leg representation. Dark colors show stance legs. The interval from 42 to 52 ms is labeled with bilaterally asymmetric abduction/adduction movements. (B) A schematic demonstration of force and torque generation by stance legs. (C,D) Temporal variation of functional length (F_L) and orientation (θ_F) of one IFL and one OEL for the trial in Fig. 5E, showing that a single IFL action is accompanied by two OEL strides. Shaded intervals denote stance periods. See Fig. S5 for more details. Asterisks in C indicate initial adduction (green). (E) The angle of body reorientation versus distance of body translation (normalized to body length; L_b) during individual stance periods, showing that the IFL actions are associated with greater body translational and rotational distances than the OEL actions. Trend lines are based on linear regression models. Point size represents stance period (see also Fig. S6). (F) Comparison of the workspaces of tarsi in the lateral and fore–aft directions between the legs of a selenopid spider (represented by IFL during a strike maneuver) and a *Blaberus* cockroach (turning during forward run). Sector radius represents the range of variation of functional length (ΔL_F) normalized by body length (L_b); sector angle represents the range of fore–aft rotations ($\Delta\theta_F$) with respect to the COM. For the cockroach, the boundaries are defined based on foot placement during turning maneuvers (the maximum $L_F \approx 0.4 L_b$; $\Delta\theta_F \approx 50$ deg; Jindrich and Full, 1999).

perceived visually or mechanically (e.g. through substrate vibrations or air currents) and then used to discriminate the position of prey. The strike maneuvers consisted of actively regulated turn-and-reach movements, with acceleration and deceleration phases, directed toward prey. Thus, the spiders used both orientation and distance cues of prey when generating the strikes. Also, the spiders struck more distantly located prey with higher speeds and maintained a strike period under 120 ms. Successful strikes must be faster than the prey's escape response (e.g. crickets respond to simulated attacks with a mean latency of 87–191 ms; Tauber and Camhi, 1995), and selection for speed may have shaped how these spiders strike farther and more posteriorly oriented prey (see also below).

These strikes are highly transient maneuvers with zero initial and end speeds, and are thus dynamically distinct from other turning maneuvers performed during forward running or with small COM displacement. The generation of these maneuvers depends on a series of biomechanically coupled, highly specialized morphological and behavioral features of the legs (see below). Our study did not address the possible damping and elastic energy storage at leg joints, but both mechanisms may facilitate the generation of strikes. For example, release of stored energy may help generate the initial accelerations, and both mechanisms likely assist with the deceleration processes. Moreover, the selenopid spiders' strike maneuvers represent some of the fastest turning rotations in multi-legged animals, with angular accelerations and speeds of the same order of magnitude as some rapid aerial maneuvers (e.g. the peak angular acceleration is $\sim 3\times10^5$ deg s^{-2} and $\sim 2\times10^5$ deg s^{-2} in fruit flies and magnificent hummingbirds, respectively; Muijres et al., 2014; Cheng et al., 2016a,b). Subsequent studies may compare extreme maneuvers under different contexts to understand the limiting factors (e.g. body size, neural delay and the efficiency of energy release) underlying animals' torsional maneuverability in general.

Journal of Experimental Biology (2018) 221, jeb166512. doi:10.1242/jeb.166512

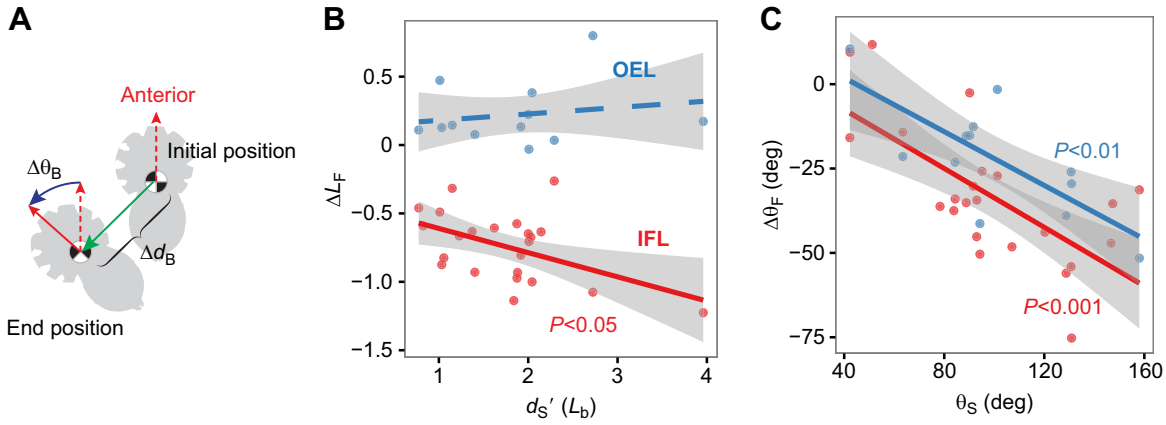

Fig. 7. Correlation between body maneuvers and leg reconfigurations. (A) Configuration of body maneuver in the horizontal plane. $\Delta\theta_B$, angle of reorientation; Δd_B, distance of COM translation. (B) Total body translation [$d_S'(L_b)$] is significantly correlated with the strain of IFL but not with that of OEL. (C) Total body reorientation (θ_S) is significantly correlated with the total rotational angles of IFL and OEL ($\Delta\theta_F$). For trials with more than one OEL stance, the sum of the amplitude from all strides was used. Trend lines are based on generalized linear regression models. Dashed line in B represents the lack of significant correlation (P>0.05).

Adaptive gait configuration for omnidirectional strikes

The success of omnidirectional strikes also depends on the effective gait configuration. The spiders partitioned their eight legs to enable the generation of momenta and regulation of whole-spider inertia. For the stance legs, the spiders adopted a bilaterally asymmetric gait, with 1–2 IFL aiming at prey and 0–3 OEL assisting at the trailing side of the strike. With a radially symmetric leg posture, the spiders can target any direction by configuring this gait using any of the eight legs as IFL. In other words, the radially aligned leg pairs form a ready-to-fire system that can immediately generate the strikes without reconfiguration. These results support our hypothesis about gait optimization. Additionally, each leg performed one of three possible actions (IFL, OEL and AAL) to drive the strikes. Future studies should investigate how the organization of joints, musculature and ambush postures together ease the immediate generation of large ground reaction forces and moments.

Functional significance of laterigrade legs for turning maneuvers

The generation of omnidirectional strikes depends on the effective use of long, laterigrade legs. The legs are used to drive turns over wide linear and angular distances within single stances. The laterigrade morphology allows the rotation of trochanter and FP joints to generate a wide range of movements in the lateral direction, thus providing a large workspace of the tarsus in the horizontal plane. This freedom of motion allows the body to rotate and translate across wide linear and angular distances relative to the tarsus that is anchored on the substrate. Thus, the spider can continuously regulate the generation of ground reaction forces and moments while the body is translating along the linear trajectory. With a reduced number of strides, the control effort for coordinating multiple legs through multiple strides can be significantly reduced. This utility shows greater capability of regulating body maneuvers over a large workspace within the plane of maneuvering (e.g. the horizontal plane for turning maneuvers) than legs with a relatively small workspace in the lateral direction (Fig. 6F). For example, the MI (i.e. the ratio of body reorientation angle to the deflection of COM linear speed during a single stance) of legs in forward-running cockroaches ranges from approximately −0.4 to approximately 1.1 (i.e. leg effectiveness number; Jindrich and Full, 1999), which is much smaller than those of selenopid spider legs and may represent a different utility for maneuvering during forward movements.

The two types of stance leg actions (IFL and OEL) exploited the laterigrade design to drive the maneuvers. In strikes that were driven by a single IFL, the IFL generated a large traction force and a rotational moment throughout the acceleration phase of the strike (Fig. 6B). This configuration has a center of pressure in the leading position of the heading of the body's linear momentum and is thus dynamically stable. The moment associated with the traction force provides stability against potential perturbation. Furthermore, IFL and OEL may dynamically interact when driving the strikes together. The kinematic correlation between body motion and leg reconfigurations (Fig. 7) suggest that the linear component of strike maneuvers was primarily regulated by the IFL adduction and the rotational component is regulated through the asymmetric rotation of both leg groups. The greater variation in angular acceleration versus linear acceleration (Fig. 4C) likely reflects these interactions. During the acceleration phases, if the IFL generates a traction force in the leading side of COM translation, the OEL likely assists with linear and angular impulses on the trailing side. Future measurements of leg-specific forces will help to explain these inter-leg interactions as well as the overall dynamic stability when multiple stance legs are used.

Arachnids generally use muscles to drive joint flexion and use hydraulic pressure to drive joint extension (Shultz, 1989; Weihmann et al., 2012). Future examination of selenopid spiders' leg musculature will help to understand the adaptations underlying the powerful leg adductions. Whole-leg reconfigurations were the main focus in this study, and incorporating the dynamics of stance-specific ground reaction forces and joint rotations can help to further understand the coordination between legs, interactions among leg joints, and the relative contributions between hydraulic extension, muscular flexion and possibly elastic elements (Spagna and Peattie, 2012; Sensenig and Shultz, 2003). Also, effective adhesion on the substrate for frictional force generation is critical for these strikes, and future studies may also examine potential morphological adaptations for strong adhesion.

The spiders also exploited the wide range of leg movements in the lateral direction for inertial regulation. They used rapid leg adductions to enhance rotational speed. The underlying mechanism is analogous to a similar technique used in figure skating – pulling the arms and the free leg toward the torso to accelerate spinning speed. However, changing leg posture to alter the moment of inertia and regulate torsional maneuverability may be more commonly seen in

Journal of Experimental Biology (2018) 221, jeb166512. doi:10.1242/jeb.166512

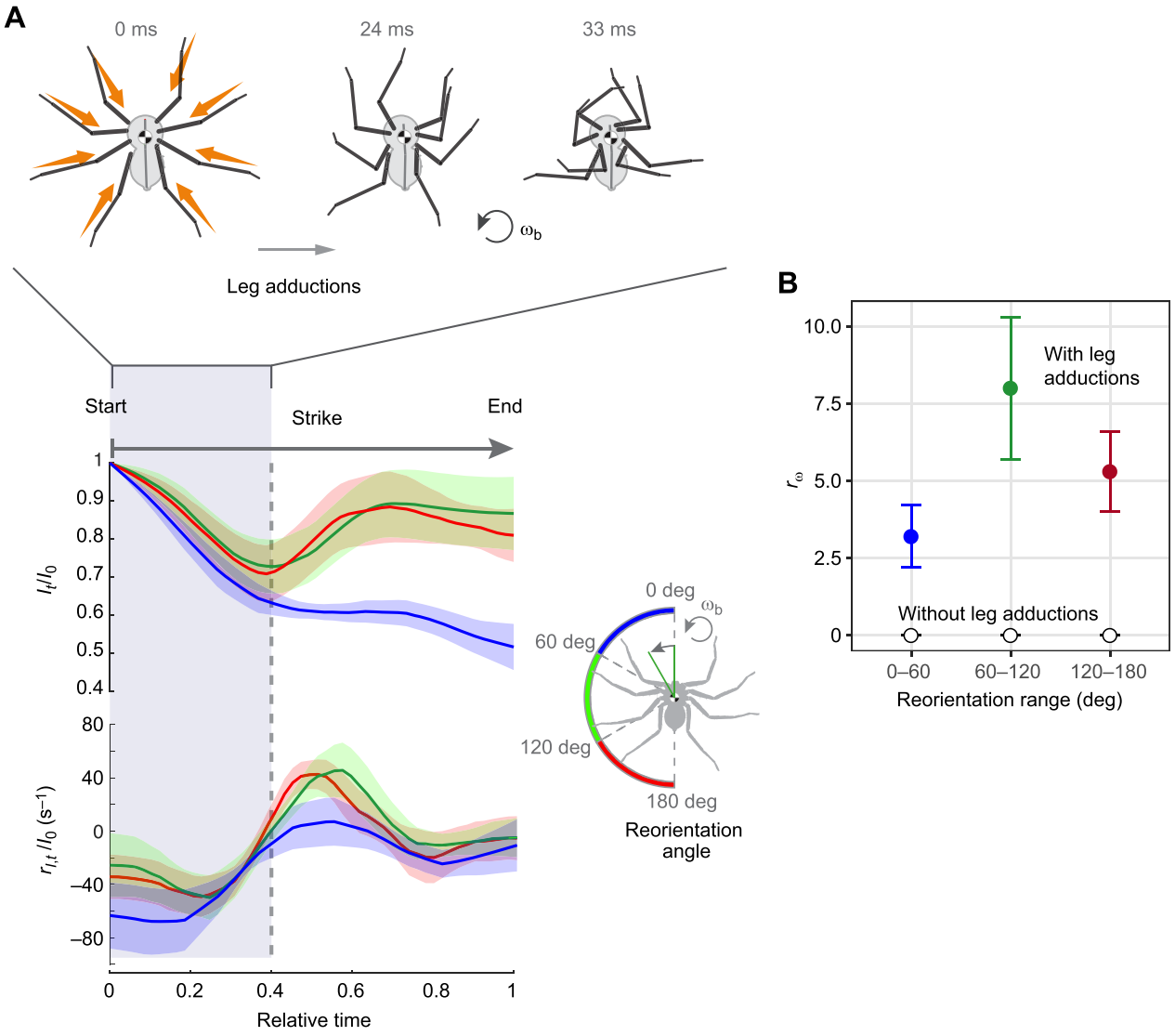

Fig. 8. Rapid leg adductions enhance the speed of reorientation. (A) Top: a sequence of leg adductions during the early phase of a strike. Legs are represented by line segments based on 3D kinematics in top view. The body orientation is fixed for clarity. Bottom: temporal variations of moment of inertia (normalized to initial values, I_t/I_0) and the rate of change of moment of inertia (normalized to initial values, $r_{I,t}/I_0$). Colors represent three ranges of body reorientation angle. Binning was used to demonstrate the variation of moment of inertia dynamics with respect to the angular distance of the prey (0–60 deg, *N*=7 trials; 60–120 deg, *N*=13; 120–180 deg, *N*=12). Shaded curves are means±s.e.m. (B) Rotation speed enhancement ratio ($r\omega$) calculated based on spider kinematics during the initial 40% of the strike period (see Appendix, 'Derivation of rotational speed enhancement by leg adductions'). Values are means±s.e.m.

rapid aerial rotations (e.g. orchid bees extend their legs to increase the moment of inertia and stabilize against turbulence-induced rolling; Combes and Dudley, 2009). Because the acceleration enhancement level is proportional to the rate of moment of inertia reduction, the effectiveness of leg adduction is determined by leg size, leg mass and the rate of adduction in the radial direction toward the COM. Thus, the radially symmetric leg alignment enhances the efforts of leg adduction by (1) allowing for efficient moment of inertia reduction and (2) maintaining a relatively consistent COM position with respect to the body frame. The rapid leg adductions can significantly reduce the overall time expenditure of maneuvers, and the evolution of this behavior is presumably coupled with the evolution of greater power release for faster strikes. These results also suggest that the radially symmetric alignment and long leg lengths are important morphological adaptations for inertia regulation during rapid rotations.

This study demonstrates the utility of long, laterigrade legs using descriptive results. Our initial hypotheses were generally supported, but further research is needed to test whether legs of alternative designs are less capable of performing these strike maneuvers. This may be conducted using theoretical modeling of alternative leg postures and examination of leg utility for tight, rapid turns in arthropods with other leg postures. From a bioengineering perspective, multi-legged robots may adopt similar leg designs and control tactics to perform tight, rapid turns (e.g. for rapid reorientation within confined spaces). In particular, incorporation of sprawled, jointed legs can help to more effectively achieve rapid turning maneuvers, and controlled leg adduction/abduction can be used to regulate rotational speed.

Ecological and evolutionary significance

Omnidirectional strike capability is likely an adaptation for ambushing on open surfaces, where prey may approach from different directions. Also, rapid maneuvers may help animals escape from predators (e.g. birds and lizards) with quick and unpredictable

turns and runs. The rapidity and robustness of these strikes may allow the spiders to ambush on surfaces of various inclines, including vertical and inverted surfaces (e.g. tree trunks, rock walls and ceilings of houses and caves), and this may partly explain their ability to inhabit diverse habitats (Crews, 2011; Crews and Harvey, 2011). From an evolutionary perspective, the body plan and omnidirectional strike capability in selenopid spiders are secondarily derived from less-specialized ancestral forms (Spagna and Peattie, 2012; Kropf, 2013). Similar maneuvering capabilities exist in other spider lineages that have convergently evolved a similar body plan (e.g. Trochanteriidae). Correlating body and leg morphology, hunting behavior and habitat information within a phylogenetic context will elucidate how these factors contribute to the evolution of omnidirectional strikes. Finally, selection for extreme performance, especially in the context of predator–prey interactions, may have significantly influenced the evolution of the arthropod musculoskeletal framework for locomotion. Our work suggests that an anteroposteriorly condensed body with long, laterigrade legs is adapted for fast turning maneuvers and provides insights for addressing the diversity of arthropod body plans, e.g. the repeated transitions from a long, slender body with short legs to an anteroposteriorly shortened body with long, laterigrade legs, on the arthropod tree of life (Regier et al., 2010).

APPENDIX

Scaling of maneuver momentum ratio

Because both linear and angular speeds are positively correlated with corresponding distances, as are the average linear and angular momentum, Eqn 8 can be re-written as:

$$\mathrm{MMR} = \frac{I\theta_S T^{-1}}{m d_S T^{-1}} = \frac{I\theta_S}{m d_S}, \tag{A1}$$

where MMR is maneuver momentum ratio, T is strike period, θ_S is angle of body reorientation and d_S is the linear distance traveled by the COM. Assuming the spiders are isomorphic, i.e. moment of inertia scales with the square of body length ($I \propto L_b^2$), we expected:

$$\mathrm{MMR} \propto \frac{\theta_S}{d_S} L_b^2, \tag{A2}$$

which indicates that MMR scales with the square of body length times the ratio of angular reorientation to linear distance (Fig. S2).

Gait configuration

The spiders exhibited various combinations of inside flexion leg (IFL) and outside flexion leg (OEL) regardless of prey distance (Fig. S3), which is mainly due to the large variations in which legs were chosen as OEL. OEL was performed by legs II, III and IV in three combinations: legs II+III+IV, legs II+IV and legs III+IV; the number of OEL strides varied between 0 and 5. Based on multiple regression models using the stride number as a continuous variable and the OEL combination as a categorical variable, we found that the number of OEL strides and the combinations of OEL were not correlated with the linear distance of prey to the spider COM (d_S) and the angular distances of prey with respect to the anterior direction of the spider (θ_S). The variability of OEL choice is not fully understood. From a control perspective, this may suggest variable motor patterns underlying the target-oriented and relatively more predictable strike performances.

Kinematics of stance legs

The intersection angles of the functional plane of each joint with respect to the horizontal plane were as follows: (1) femur–patella joint: 62±2 deg for IFL (N=32) and 57±6 deg for OEL (N=24); CTF joints: 47±4 deg for IFL and 60±6 deg for OEL (means±s.e.m.).

Fig. S4 shows the three-dimensional joint kinematics of stance legs. Fig. S5 shows more details of the kinematics of stance leg reconfigurations. Fig. S6 shows the templates of deformation in IFL and OEL. The within-stance changes in functional length and orientation are correlated regardless of leg pairs, showing a template of action depending on whether the leg acts as an IFL or OEL.

Derivation of rotational speed enhancement by leg adductions

All legs performed adductions during the initiation of strikes and the non-stance legs maintain the adducted posture mid-maneuver. The initial leg adductions induced ~25% reduction of the mass moment of inertia about a vertical rotational axis during the initial 40% of the strike period (i.e. 0–0.4 T; Fig. 8A). Here, we address how a rapid reduction of moment of inertia enhances the speed of body rotation. Assuming a constant angular impulse and a constant reduction of moment of inertia throughout the acceleration phase, we compare the rotational speed between a simplified model derived from the spider kinematics and a control model without leg adduction. Based on the balance of angular momentum, the equation of rotational motion is:

$$\ddot{\theta} I + \dot{\theta}\dot{I} = \tau, \tag{A3}$$

where τ is reorientational torque, θ is angular displacement and I is moment of inertia. After solving Eqn A3, we can describe the angular distance traveled by time t as:

$$\theta_t = \exp\left(-\frac{r_I t}{2I_0} + \frac{t}{2}\sqrt{\left(\frac{r_I}{I_0}\right)^2 + \frac{4\tau}{I_0}}\right), \tag{A4}$$

where r_I is the rate of change of I and I_0 is the initial value of I prior to leg adduction. Eqn A4 can be re-written as:

$$\theta_t = \exp\left(\frac{-t}{2}\bar{r}_I + \frac{t}{2}\sqrt{\bar{r}_I^2 + 4\alpha_0}\right), \tag{A5}$$

where $\bar{r}_I = r_I/I_0$ is r_I normalized by the initial value (see Fig. 8A), and $\alpha_0=\tau/I_0$ is the angular acceleration at t=0 for the simplified model and is equal to the acceleration of the control model. To evaluate the degree of rotational speed enhancement by leg adduction, we compare the rotational speed achieved by the simplified model with the parameters found in spiders (I_0, $\bar{r}_I$ and α_0) to that of the control model. We first estimate α_0 by applying the mean $\bar{r}_I$ and θ_t throughout 0–0.4 T to Eqn A5. Next, we calculate the mean rotational speed of the simplified model ($\bar{\omega}_t=\theta_t/t$) and that of control model ($\bar{\omega}_t'=0.5\alpha_0 t$) during 0–0.4 T. Lastly, we define $r_\omega=\bar{\omega}_t/\bar{\omega}_t'$ as the rotation speed enhancement ratio, and it represents the ratio of enhanced angular speed to that of the control model.

Acknowledgements

We thank Zheyuan Xu and Alan Sanders for helping with data analyses and morphological data collection, and Jillian Cowles, Nicole VanderSal-Jensen and Lauren Esposito for providing some specimens. We also thank Chen Li, Talia Moore and Bo Cheng for comments on the manuscript, and Robert Full, Thomas Libby, Jerome Casas, Joe Spagna and Shai Revzen for insightful discussion. We further acknowledge research facilities provided by the Center for Interdisciplinary Biological Inspiration in Education and Research (CiBER) at UC-Berkeley.

Competing interests

The authors declare no competing or financial interests.

Author contributions

Conceptualization: Y.Z., S.C.; Methodology: Y.Z., S.C.; Software: Y.Z.; Validation: Y.Z., S.C.; Formal analysis: Y.Z.; Investigation: Y.Z.; Resources: Y.Z., S.C.; Data curation: Y.Z., S.C.; Writing - original draft: Y.Z.; Writing - review & editing: Y.Z., S.C.; Visualization: Y.Z.; Supervision: S.C.; Project administration: Y.Z., S.C.

Funding

This research received no specific grant from any funding agency in the public, commercial, or not-for-profit sectors.

Data availability

The datasets have been deposited in the Open Science Framework repository: https://osf.io/h9b4t/?view_only=bd3fa03865ad4fcd8b887b778c474c25

Supplementary information

Supplementary information available online at http://jeb.biologists.org/lookup/doi/10.1242/jeb.166512.supplemental

References

Cheng, B., Tobalske, B. W., Powers, D. R., Hedrick, T. L., Wethington, S. M., Chiu, G. T. C. and Deng, X. (2016a). Flight mechanics and control of escape manoeuvres in hummingbirds. I. Flight kinematics. *J. Exp. Biol.* **219**, 3518-3531.

Cheng, B., Tobalske, B. W., Powers, D. R., Hedrick, T. L., Wang, Y., Wethington, S. M., Chiu, G. T.-C. and Deng, X. (2016b). Flight mechanics and control of escape manoeuvres in hummingbirds. II. Aerodynamic force production, flight control and performance limitations. *J. Exp. Biol.* **219**, 3532-3543.

Combes, S. A. and Dudley, R. (2009). Turbulence-driven instabilities limit insect flight performance. *Proc. Natl. Acad. Sci. USA* **106**, 9105-9108.

Crews, S. C. (2011). A revision of the spider genus Selenops Latreille, 1819 (Arachnida, Araneae, Selenopidae) in North America, Central America and the Caribbean. *ZooKeys* **105**, 1.

Crews, S. C. and Harvey, M. S. (2011). The spider family Selenopidae (Arachnida, Araneae) in Australasia and the Oriental Region. *Zookeys* **99**, 1-104.

Crews, S. C., Wienskoski, E. and Gillespie, R. G. (2008). Life history of the spider *Selenops occultus* Mello-Leitão (Araneae, Selenopidae) from Brazil with notes on the natural history of the genus. *J. Nat. Hist.* **42**, 2747-2761.

deVries, M. S., Murphy, E. A. K. and Patek, S. N. (2012). Strike mechanics of an ambush predator: the spearing mantis shrimp. *J. Exp. Biol.* **215**, 4374-4384.

Franklin, R., Bell, W. J. and Jander, R. (1981). Rotational locomotion by the cockroach *Blattella germanica*. *J. Insect Physiol.* **27**, 249-255.

Full, R. J. (1997). Invertebrate locomotor systems. In *The Handbook of Comparative Physiology*, Vol. 2 (ed. W. H. Dantzler), pp. 853-930. Oxford: Oxford University Press.

Full, R. J., Kubow, T., Schmitt, J., Holmes, P. and Koditschek, D. (2002). Quantifying dynamic stability and maneuverability in legged locomotion. *Integr. Comp. Biol.* **42**, 149-157.

Jindrich, D. L. and Full, R. J. (1999). Many-legged maneuverability: dynamics of turning in hexapods. *J. Exp. Biol.* **202**, 1603-1623.

Kardong, K. V. (1986). The predatory strike of the rattlesnake: when things go amiss. *Copeia* **1986**, 816-820.

Kropf, C. (2013). Hydraulic system of locomotion. In *Spider Ecophysiology* (ed. W. Nentwig), pp. 43-56. Berlin: Springer.

Manton, S. M. (1973). Arthropod phylogeny—a modern synthesis. *J. Zool.* **171**, 111-130.

Moore, T. Y. and Biewener, A. A. (2015). Outrun or outmaneuver: predator-prey interactions as a model system for integrating biomechanical studies in a broader ecological and evolutionary context. *Integr. Comp. Biol.* **55**, 1188-1197.

Muijres, F. T., Elzinga, M. J., Melis, J. M. and Dickinson, M. H. (2014). Flies evade looming targets by executing rapid visually directed banked turns. *Science* **344**, 172-177.

Murray, R. M., Li, Z. and Sastry, S. (1994). *A Mathematical Introduction to Robotic Manipulation*, Boca Raton: CRC Press.

Regier, J. C., Shultz, J. W., Zwick, A., Hussey, A., Ball, B., Wetzer, R., Martin, J. W. and Cunningham, C. W. (2010). Arthropod relationships revealed by phylogenomic analysis of nuclear protein-coding sequences. *Nature* **463**, 1079-1083.

Schindelin, J., Rueden, C. T., Hiner, M. C. and Eliceiri, K. W. (2015). The ImageJ ecosystem: an open platform for biomedical image analysis. *Mol. Reprod. Dev.* **82**, 518-529.

Sensenig, A. T. and Shultz, J. W. (2003). Mechanics of cuticular elastic energy storage in leg joints lacking extensor muscles in arachnids. *J. Exp. Biol.* **206**, 771-784.

Shultz, J. W. (1989). Morphology of locomotor appendages in Arachnida: evolutionary trends and phylogenetic implications. *Zool. J. Linnean. Soc.* **97**, 1-55.

Spagna, J. C. and Peattie, A. M. (2012). Terrestrial locomotion in arachnids. *J. Insect Physiol.* **58**, 599-606.

Tauber, E. and Camhi, J. (1995). The wind-evoked escape behavior of the cricket *Gryllus bimaculatus*: integration of behavioral elements. *J. Exp. Biol.* **198**, 1895-1907.

Walker, J. A. (1998). Estimating velocities and accelerations of animal locomotion: a simulation experiment comparing numerical differentiation algorithms. *J. Exp. Biol.* **201**, 981-995.

Weihmann, T., Günther, M. and Blickhan, R. (2012). Hydraulic leg extension is not necessarily the main drive in large spiders. *J. Exp. Biol.* **215**, 578-583.

Wootton, R. J. (1999). Invertebrate paraxial locomotory appendages: design, deformation and control. *J. Exp. Biol.* **202**, 3333-3345.

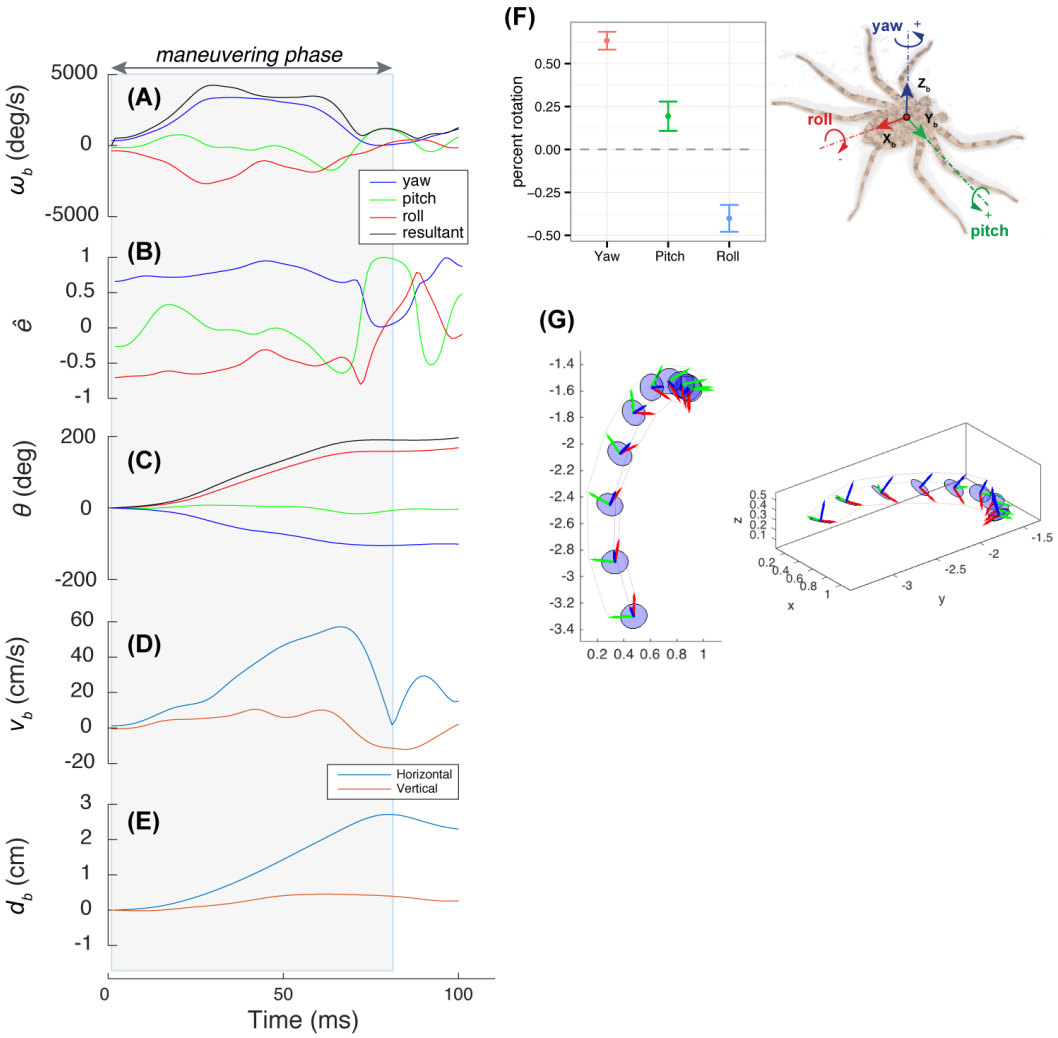

Fig. S1 Body kinematics of a strike maneuver. (A-E) Rotational and translational dynamics of one trial (θ_p~160°). The shaded interval highlights the maneuvering phase during which period the spider completes one smooth rotation. (A) Rotational velocities, showing a major peak of speed mid-maneuver. (B) Temporal shifts in the orientation of the rotational axis with respect to body-fixed frame. (C) Angular distances traveled by each principle rotation. (D) Translational velocity of body frame. (E) Linear distance travelled by body frame. (F) Relative proportions of each principal rotation during the maneuvering phase (means±s.e.m.). The spider body mainly performs positive yaw and negative roll to reorient, which is accompanied by positive (nose-up) pitch. (G) 3D reconstruction of body frame orientation during the strike maneuver of the same trial in (A-E), where the disc represents the X_b-Y_b plane, and red arrows represent positive X_b direction. Left, top view; right, oblique view.

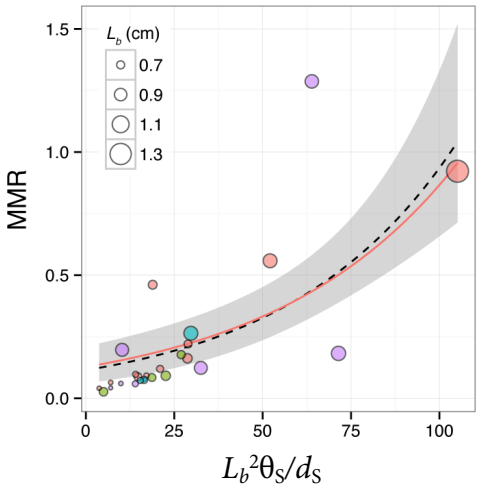

Fig. S2 Maneuver momenta ratio (MMR) plotted against $(\boldsymbol{L_b^2}\ \boldsymbol{\theta}_s)/\boldsymbol{d}_s$, showing that the spiders generate greater energy output when striking farther and more posteriorly oriented prey. $\boldsymbol{L_b}$, body length; $\boldsymbol{\theta}_s$, angle of reorientation; $\boldsymbol{d}_s$, linear distance of prey to initial spider COM.

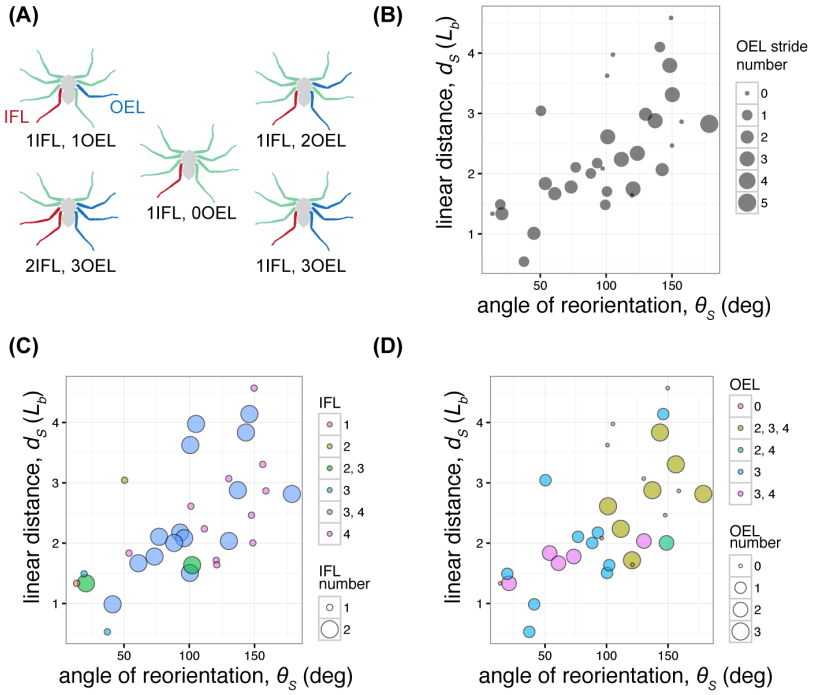

Fig. S3 Gait patterns of strike maneuvers. (A) Demonstrations of various combinations of IFL and OEL. (B) The number of OEL strides plotted against linear distance ($\boldsymbol{d_S}$) and angular distance ($\boldsymbol{\theta_S}$). Based on generalized linear regression models the number of OEL strides is not correlated with either distances. (C) Different combinations of IFL plotted against $\boldsymbol{d_S}$ and $\boldsymbol{\theta_S}$. Colors represent different IFL combinations; point size represents the number of IFL. (D) Different OEL combinations mapped against $\boldsymbol{d_S}$ and $\boldsymbol{\theta_S}$. Based on generalized linear regression models, the number and combinations of IFL and OEL are not correlated with $\boldsymbol{d_S}$ and $\boldsymbol{\theta_S}$. Kinematics is based on left-turn configuration (see Methods).

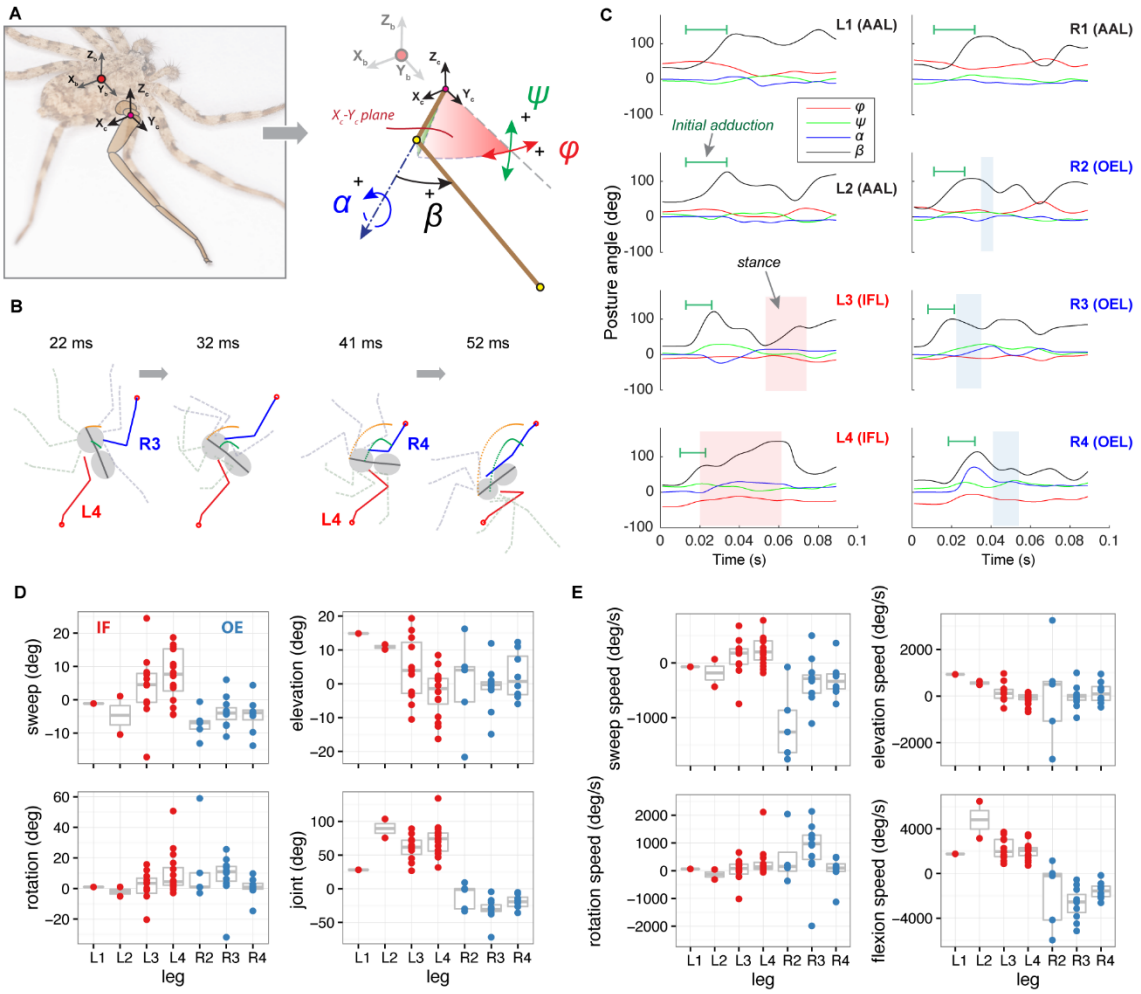

Fig. S4 Three-dimensional leg joint kinematics. (A) Configuration of leg posture angles, demonstrated with leg III. The coxa-fixed coordinate frame has principal axes parallel to those of the body-fixed frame. Four angles describe leg posture: ϕ, sweep angle; ψ, elevation angle; α, rotation angle; β, FP-joint angle. (B) Mid-maneuver sequences of body and leg postures in top view. (C) Dynamics of leg posture angles from the same trial shown in (B). Green segmented lines show initial flexion of FP-joints at the beginning of the maneuver. Shaded areas represent stance. (D) Summary of amplitude of joint rotations for each posture angle for IF and OE actions. (E) Summary of joint rotation speeds for IFL and OEL actions. Kinematics is based on left-turn configuration (see Methods).

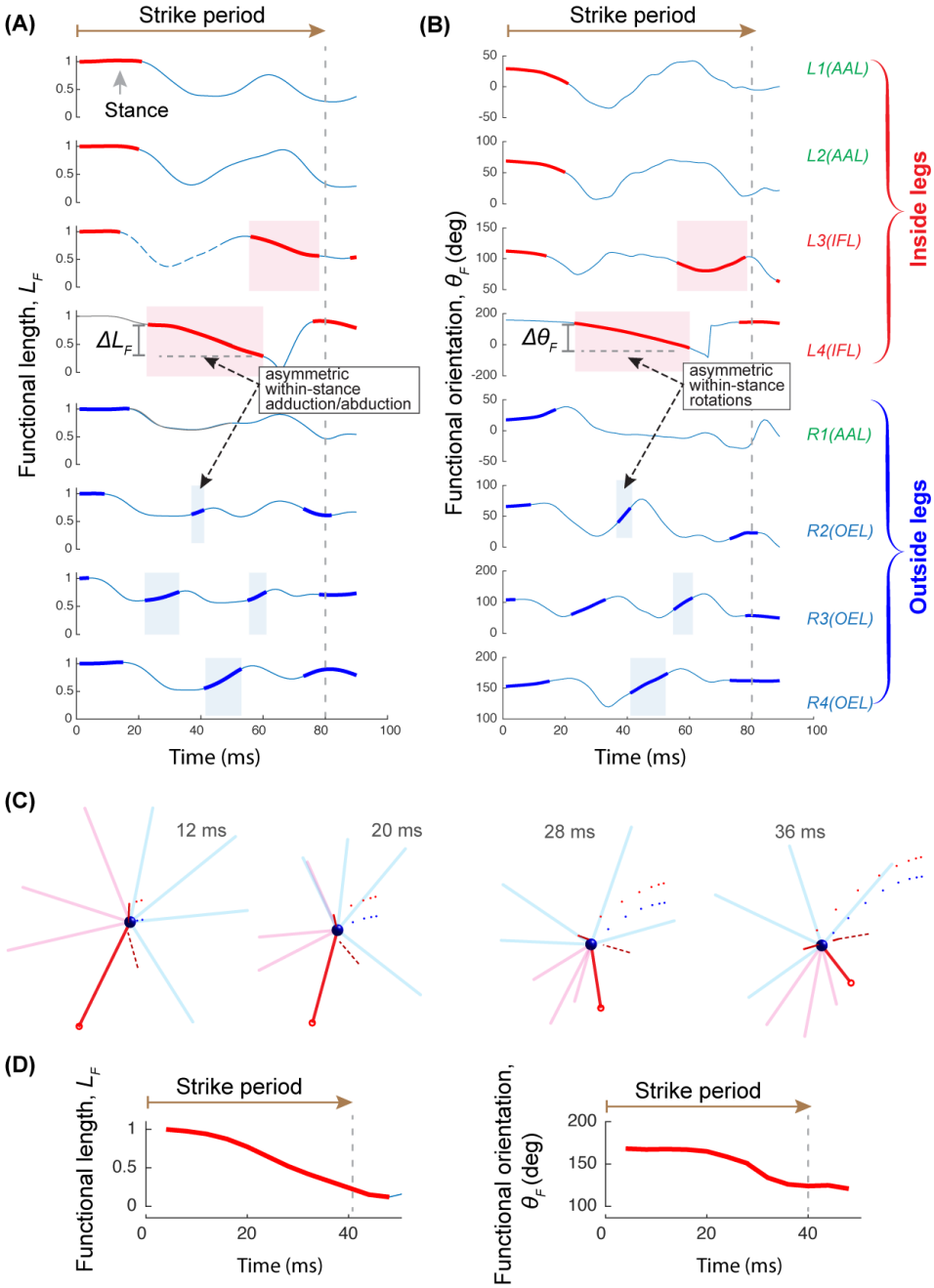

Fig. S5 Kinematics of leg deformations. (A)-(B) Dynamics of functional leg length (initial size normalized) and functional orientation ($\boldsymbol{\theta_F}$) of the same trial in Fig. 5E. Shaded intervals represent stance. Red, inside legs; blue, outside legs; thickened segments of lines represent stance. (C)-(D), Kinematics of leg deformations for a strike driven by a single IFL (left leg IV). (C) Strike sequence in functional leg representation. (D) Temporal dynamics of functional leg length (initial size normalized) and functional orientation of left leg IV. Kinematics is based on a left-turn configuration.

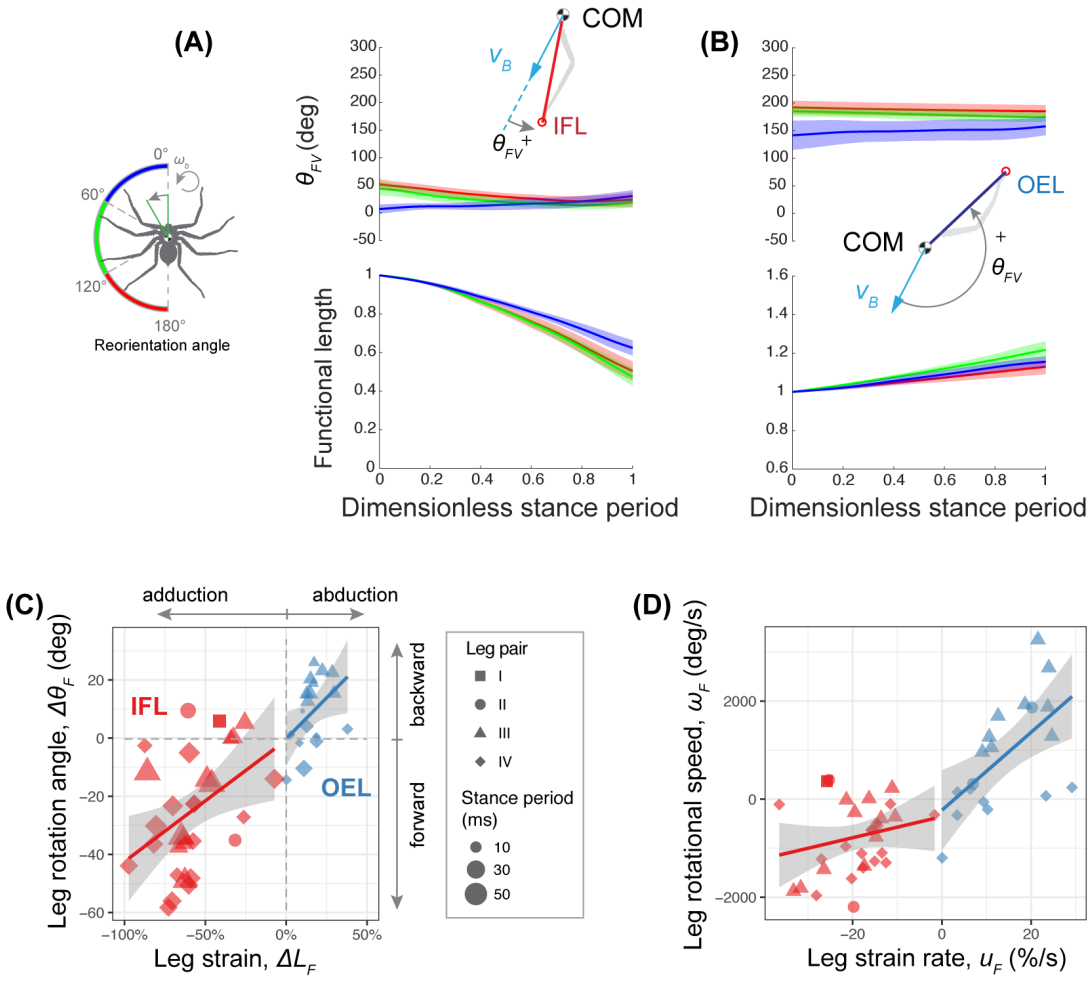

Fig. S6 Comparison of deformation kinematics between four leg pairs. (A) Dynamics of functional orientation and length variation during stance of IFL, showing shortening (i.e., adduction) and forward rotation in the leading side of COM heading. Color represents the three ranges of the total reorientation angle. $\boldsymbol{\theta_{FV}}$, leg functional orientation vs. COM velocity $\boldsymbol{v_B}$, with counter-clockwise as the positive direction. (B) Dynamics of functional length and orientation variation during stance of OEL, which performs lengthening (i.e., abduction) in the trailing side of COM velocity. (C) Correlation between the degree of abduction/adduction ($\boldsymbol{\Delta L_F}$) and rotation amplitude ($\boldsymbol{\Delta\theta_F}$), showing the coupling between abduction/adduction and rotations. Trend lines represent generalized linear models; shaded areas represent s.e.m. (D) Correlations between the rate of abduction/adduction ($\boldsymbol{u_F}$) and rotation speed ($\boldsymbol{\omega_F}$). (C) and (D) suggest kinematics templates of within-stance deformation were shared by legs playing the same roles for strike maneuver. (C) and (D), $P<0.01$ for all correlations based on a generalized linear regression model.

Tables

	L_l/L_b	L_1/L_2
Leg I	1.3 ± 0.3	1.95 ± 0.19
Leg II	1.9 ± 0.6	1.9 ± 0.22
Leg III	1.4 ± 0.3	1.99 ± 0.12
Leg IV	2 ± 0.5	1.86 ± 0.27

Table S1. Length ratio between body and leg sections. L_l/L_b, leg length to body (cephalothorax and abdomen) length ratio. L_1/L_2, length ratio of section 1 to section 2 (Fig. 2A). Values are means±s.d.

Body parts		Mass percentage
Cephalothorax		32.7 ± 4.98
Abdomen		23.3 ± 6.21
Leg I	a	0.54 ± 0.38
	b	2.84 ± 0.97
	c	6.32 ± 1.45
Leg II	a	0.51 ± 0.47
	b	3.92 ± 0.99
	c	7.91 ± 1.54
Leg III	a	0.85 ± 0.59
	b	3.48 ± 0.98
	c	7.7 ± 1.79
Leg IV	a	0.8 ± 0.54
	b	2.69 ± 1.26
	c	6.45 ± 1.54

Table S2. Mass distribution of body sections (*S. wilsoni*, *N*=5; *S. debilis*, *N*=5). Values are mass percentages with respect to total (means±S.D.). See Fig. S2 for partitioning of leg sections for mass distribution measurement. Leg sections: a, tarsus and metatarsus; b, tibia; c, femur. Mass percentages of each leg section represent single sections.

Taxa		Strike direction	Medium	Prey cues	Period	Linear speed	Linear distance	Reference
mantis shrimp	*Lysiosquillina maculata*	forward	Water	visual, chemosensory	24.98±9.68 ms		~2.2% to 6.7% L_b	deVries et al., 2012
	Alachosquilla vicina	forward	Water		3.26±0.41 ms		~25.3% to 50.1% L_b	deVries et al., 2012
	Odontodactylus scyllarus	forward	Water			14 to 23 m/s		Patek et al., 2004
snake	Shedao pit-viper (*Gloydius shedaoensis*)	forward, straight upward	Air	visual, thermal		0.5 to 2.5 m/s	>20 cm, or 25% L_b	Shine et al., 2002; Shine and Sun, 2002
	Pacific rattlesnake (*Crotalus viridis*)	forward	Air					Kardong, 1986
	Couch's garter snake (*Thamnophis couchii*)	fForward	Water	visual		1.12 m/s (mean peak speed)	2 to 12 cm, or 4% to 20% L_b	Alfaro, 2002
	Tentacled snake (*Erpeton tentaculatus*)	lateral to head	Water	mechanical	30 to 40 ms	~1.1 m/s (mean)	0.8 to 3.0 cm, or 3% to 12% L_b	Smith et al., 2002; Catania, 2009
spider	crab spider (*Misumena vatia*)	forward	Air	visual, mechanical				Morse, 1981
	trapdoor spider (*Aliatypus* sp.)	forward	Air	mechanical	30 to 130 ms		5 mm maximum	Coyle and Icenogle, 1994
	flattie spider (*Selenops* spp.)	omnidirectional (Fig. 3)	Air	visual, mechanical	52 to 116 ms	0.2 to 0.6 m/s (or 10 to 80 L_b/s)	100% to 500% L_b	present study

Table S3. Comparison of strike performance between different ambush predators. *, calculated based on data from cited literature. L_b, body length. This comparison shows flattie spiders perform fast strikes that cover angular and linear ranges greater than other ambush predators.

Taxa	***Turning performance***	***Heading angle change; longitudinal axis rotation (deg)***	***Linear speed (cm/s, L_b/s)***	***Angular speed (deg/s) (mean; maximum)***	***Curvature (cm^{-1})***	***Number of strides***	***Body length (cm)***	***Body mass (g)***	***Reference***
Death-head cockroach (*Blaberus discoidalis*)	during running	48; 40	20; 4.5	157	0.8	3.6	4.4	4.6	Jindrich and Full, 1999; Kram et al., 1997
Mite (*Paratarsotomus macropalpis*)	during running; with pivot leg	~; 103	2.4; 21	795; 1253	5.8	3.4	0.114	2.5×10^{-5} to 2.5×10^{-4}	Rubin et al., 2016
	during running; without pivot leg	~; 102	2.9; 27.4	567; 1040	3.4	4	0.106		
Fruitfly (*Drosophila melanogaster*)	tight turn	~; 100		400 (single trial)			0.25		Strauss and Heisenberg, 1990
Honeybee (*Apis mellifera*)	tight turn	~; 180		157	0.89		1.6		Zolotov et al., 1975
Flattie spider (*Selenops* spp.)	ambush turn	<10–50; 10-160	10-60; 10-80 (Fig.4)	~; ~3000 (Fig.4)	2.54±6.54 (mean±SD)	0-1 (inside leg); 0-3 (outside leg)	0.5–1.4	0.019-0.279	present study

Table S4. Comparison of turning maneuvers in arthropods. Here turning maneuver specifically refers to the reorientation of body longitudinal axis along the substrate, mostly consisting of yaw. Values were calculated based on data from the original reference if necessary. '~' represents missing data or non-applicable. This comparison also shows flattie spiders perform fast turning maneuvers with fewer strides than other animals.

Effects	Coefficients (s.e.)	*T* value	*P* value
Strike reorientational speed (deg/s)			
Prey angular distance (deg)	13.6 (1.2)	11.3	<0.001
Body size (cm)	-536.1 (213.0)	-2.5	<0.05
Body size – normalized strike linear speed (L_b/s)			
Prey linear distance (cm)	12.3 (1.6)	7.6	<0.001
Body size (cm)	-17.5 (6.2)	-2.8	<0.01

Table S5. Summary of multiple regression analyses addressing the effects of prey distance and body size to strike speed, including both angular and linear components.

Supplementary References

Alfaro, M. E. (2002). Forward attack modes of aquatic feeding garter snakes. *Functional Ecology* **16**, 204-215.

Catania, K. C. (2009). Tentacled snakes turn C-starts to their advantage and predict future prey behavior. *Proc Natl Acad Sci U S A* **106**, 11183-11187.

Coyle, F. A. and Icenogle, W. R. (1994). Natural history of the Californian trapdoor spider genus *Aliatypus* (Araneae, Antrodiaetidae). *Journal of Arachnology*, 225-255.

deVries, M. S., Murphy, E. A. and Patek, S. N. (2012). Strike mechanics of an ambush predator: the spearing mantis shrimp. *J Exp Biol* **215**, 4374-4384.

Jindrich, D. L. and Full, R. J. (1999). Many-legged maneuverability: dynamics of turning in hexapods. *J Exp Biol* **202**, 1603-1623.

Kardong, K. V. (1986). The predatory strike of the rattlesnake: when things go amiss. *Copeia* **1986**, 816-820.

Kram, R., Wong, B. and Full, R. J. (1997). Three-dimensional kinematics and limb kinetic energy of running cockroaches. *J Exp Biol* **200**, 1919-1929.

Morse, D. H. (1981). Prey capture by the crab spider *Misumena vatia* (Clerck)(Thomisidae) on three common native flowers. *American Midland Naturalist*, 358-367.

Patek, S. N., Korff, W. L. and Caldwell, R. L. (2004). Deadly strike mechanism of a mantis shrimp. *Nature* **428**, 819-820.

Rubin, S., Young, M. H., Wright, J. C., Whitaker, D. L. and Ahn, A. N. (2016). Exceptional running and turning performance in a mite. *J Exp Biol* **219**, 676-685.

Shine, R., Sun, L. -X., Fitzgerald, M., Kearney, M. and Guyer, C. (2002). Antipredator responses of free-ranging pit vipers (Gloydius shedaoensis, Viperidae). *Copeia* **2002**, 843-850.

Shine, R. and Li-Xin, S. (2002). Arboreal ambush site selection by pit-vipers *Gloydius shedaoensis*. *Animal Behaviour* **63**, 565-576.

Smith, T. L., Povel, G. D. E. and Kardong, K. V. (2002). Predatory strike of the tentacled snake (*Erpeton tentaculatum*). *Journal of Zoology* **256**, 233-242.

Strauss, R. and Heisenberg, M. (1990). Coordination of legs during straight walking and turning in *Drosophila melanogaster*. *J Comp Physiol A* **167**, 403-412.

Zolotov, V., Frantsevich, L. and Falk, D. -I. E. -M. (1975). Kinematik der phototaktischen Drehung bei der Honigbiene *Apis mellifera* L. *Journal of comparative physiology* **97**, 339-353.

Supplementary movie 1

Four sample clips of strike maneuvers.

Supplementary movie 2

Reconstructed strike maneuver sequences. For skeletal view, body and leg sections are shown as line segments; red dotted lines represent trajectories of the anterior end; black dotted lines represent trajectories of the spider's center of mass; red circles indicate substrate contact. For 'functional leg' representation, the blue sphere represents spider center of mass; red dotted lines are trajectories of the anterior end; blue dotted lines are trajectories of spider center of mass; red circles indicate substrate contact.